1951

Investigation of the feasibility of using models in harnessed circling flight for the evaluation of airplane longitudinal stability

Munk, Maximilian W.; McQueen, Kenneth T.

Princeton University

AN INVESTIGATION OF THE FEASIBILITY OF USING MODELS IN HARNESSED CIRCLING FLIGHT FOR THE EVALUATION OF AIRPLANE LONGITUDINAL STABILITY

BY

M. W. MUNK

K. T. McQUEEN

PRINCETON UNIVERSITY

AERONAUTICAL ENGINEERING LABORATORY

REPORT NO. 181

INVESTIGATION OF THE FEASIBILITY OF USING MODELS IN HARNESSED CIRCLING FLIGHT FOR THE EVALUATION OF AIRPLANE LONGITUDINAL STABILITY

TABLE OF CONTENTS

ACKNOWLEDGMENT

The authors extend their appreciation and gratitude to Professor Courtland D. Perkins for his instruction and patience, to Colonel H. L. Mack of the New Jersey National Guard for providing a flying site, and to the Johnsville Naval Air Development Center for lending Photographic equipment. Also special appreciation to Mr. Harry Ashworth, Sr., whose construction and repair of mechanical components and whose unflagging interest in this project made possible whatever success was attained.

SUMMARY

This investigation was performed at Princeton University in the period from February, 1951 to June, 1951.

The original intention was an experimental investigation of the feasibility of using a powered model in harnessed circling flight to evaluate the longitudinal stability of a full-scale airplane. The airplane selected was the Cessna 140 two-place light airplane, since its stability derivatives and other parameters had been determined and were at hand. A one-tenth scale flying model was constructed.

The method of attack was to have been as follows:

A. Determination of stick-fixed neutral point, N_o from steady-state flight tests.

B. Experimental determination of the model's frequency response $\frac{\theta}{\delta}$ by obtaining a transient response of θ to an elevator pulse input and converting this to the frequency response by the method outlined in Reference 11.

C. Correlation of A and B with theory.

No quantitative data were obtained for A and B due to mechanical difficulties and lack of time. Sufficient qualitative data were obtained, however, to show agreement between the model's transient response and that predicted by theory; to point up several difficulties peculiar to this type of testing; and to indicate recommendations for further development of the method.

It was found that the scale chosen gave too small a model from considerations of required mechanical installations and dynamic similarity.

Transient response tests of relatively short duration were found to be the only feasible type due to the presence of wake disturbances.

INTRODUCTION

With the increasing number of new and radically different configurations of airplanes being introduced for sonic, transonic and convertaplane purposes it seems that some method of evaluating the low-speed longitudinal stability characteristics in unaccelerated forward flight is desirable prior to fixing a design. This could most easily be done in model form. A technique such as this would allow the inertia forces on the model to be interpreted to full scale results and would also be valuable in determining gust loadings.

The Air Materiel Command at Wright Patterson AFB established a test facility which gave promise of yielding such data.

An analytical study (Reference 5) was made by AMC. From this it was concluded that certain of the longitudinal stability characteristics could be evaluated, and that even where the dynamic stability of the phugoid mode was greatly modified by the harnessing forces on the model, the model response could be related to full scale response by certain mathematical operations. Unfortunately the test facility was decommissioned before any data were taken to substantiate the above conclusions, and at the time of commencement of this investigation, had not been re-established.

This facility made use of powered models flown in harnessed circling flight; a type of flight known as "control-line flying" which is used as a sport or hobby by certain of the general public.

It was the purpose, therefore, of the present investigation to provide a limited amount of information on which to evaluate harnessed circling flight of models as a testing method, and to establish, if possible, testing techniques which will complement the method. To this end a one-tenth

scale model of the Cessna 140 light two-place airplane constructed. Reasons dictating choice of this airplane were that complete static flight tests and wind tunnel tests of the Cessna 140 have been previously made here by the Aeronautical Engineering Department of Princeton University and therefore complete data were available. This investigation was limited to comparing the neutral point, as obtained from level flight testing of the model, with the neutral point from flight test of the full-scale airplane; and comparing the frequency response of the model's pitch angle to that obtained from the equations of motion of the airplane. The experimental frequency response was to be obtained from the analysis of the transient response to a triangular pulse of elevator deflection.

These limitations were dictated by lack of facilities, funds and time.

The data were to be obtained from static stability flight tests of the model with three center-of-gravity positions and from transient response tests at one center-of-gravity position (27.8% mac).

It is believed that this investigation is the only one of its kind to date. Although the final results may not be conclusive due to rather primitive equipment, it may indicate a method and provide a part of the information necessary for a complete analysis of the method, which of course, requires numerous tests on many more of the longitudinal stability aspects.

SYMBOLS AND ASSUMPTIONS

AR - Wing aspect ratio

AC - Aerodynamic center of the wing

$a_o = \left(\frac{dC_L}{d\alpha}\right)_o$ - Slope of the lift curve of the wing (two dimensional) (per degree)

$a_w = \left(\frac{dC_L}{d\alpha}\right)_w$ - Slope of the lift curve of the wing (three dimensional) (per degree)

$a_t = \left(\frac{dC_L}{d\alpha}\right)_t$ - Slope of the lift curve of the tail (three dimensional) (per degree)

b - Wing span -- feet

c - Mean Aerodynamic Chord of the Wing -- feet

C.G. - Center of Gravity

$C_{D_w} = \frac{D_w}{\frac{1}{2}\rho V^2 S}$ - Wire drag coefficient

$C_D = \frac{D + D_w}{\frac{1}{2}\rho V^2 S}$ - Drag Coefficient

C_D^* - Effective drag coefficient $(C_D - C_T)$

$C_T = \frac{T}{\frac{1}{2}\rho V^2 S}$ - Thrust coefficient

C_{D_f} - Parasite drag coefficient

C_{D_i} - Induced drag coefficient

$C_L = \frac{L}{qS}$ - Lift coefficient

$C_{L_t} = \frac{L_t}{qS}$ - Lift coefficient of the tail

$C_m = \frac{M}{qSc}$ - Pitching Moment coefficient of the airplane

$C_{D_\alpha} = \frac{dC_D}{d\alpha}$ - Change in drag coefficient with change in angle of attack.

$C_{D_\alpha}^* = \frac{dC_D^*}{d\alpha}$ - Change in effective drag coefficient with change in angle of attack.

$\Delta\phi$ - Angle between flying wires and datum plane

$C_{L_\alpha} = \frac{dC_L}{d\alpha}$ - Change in lift coefficient with change in angle of attack -- per radian

$C_{m_\alpha} = \frac{dC_m}{d\alpha}$ - Change in pitching moment coefficient with change in angle of attack -- per radian

$C_{m_{d\alpha}} = \frac{dC_m}{d\left(\frac{d\alpha}{dt/T}\right)}$ - Change in pitching moment coefficient with rate of change of angle of attack with respect to t/T

$C_{m_{d\theta}} = \frac{dC_m}{d\left(\frac{d\theta}{dt/T}\right)}$ - Change in pitching moment coefficient with rate of change of pitch angle with respect to t/T

$C_{m_\delta} = \frac{dC_m}{d\delta}$ - Change in pitching moment coefficient with change in elevator angle.

D - Total drag of the airplane -- lbs

d - Differential operator

e - 0.869 - Airplane efficiency factor

F - Centrifugal force in level flight

$f = \frac{F}{R}\frac{\tau}{\rho V S}$ - Non-dimensional line force

g - Acceleration due to gravity -- 32.2 ft/sec^2

$h = \frac{2(k_y)^2}{\mu c^2}$ - Non-dimensional inertia parameter

$I_y = m(k_y)^2$ - Airplane moment of inertia about the Y axis -- slug ft^2

i or j - $\sqrt{-1}$

mac - Mean aerodynamic chord -- per cent

k_y - Radius of gyration about the Y axis -- ft

L - Total lift of the airplane -- lbs

ℓ_t - Tail length (airplane CG to AC horizontal tail) -- feet

M - Moment about the Y axis -- lb-ft

m - Mass of airplane -- slugs

mph - Miles per hour

N_o - Stick-fixed neutral point

n - Normal acceleration (along the Z axis at the CG) -- "G" units

P - Period of oscillation -- seconds

$q = \frac{1}{2}\rho V^2$ - Dynamic pressure

R - Radius of flight circle.

S - Wing area -- ft^2

S_t - Horizontal tail area -- ft^2

$T_{1/2}$ - Time to damp to 1/2 amplitude -- sec

t - Time -- sec

u - Speed ratio $\frac{\Delta V}{V}$, incremental change in airspeed divided by airspeed

V - True airspeed -- ft/sec

$\overline{V} = \frac{S_t l_t}{S c}$ - Volumetric coefficient of the tail

W - Gross weight (average) -- pounds

GREEK SYMBOLS

α - Angle of attack of wing -- degrees

α_t - Angle of attack of the horizontal tail -- degrees

δ_e - Elevator deflection -- degrees

ϵ - Angle of downwash -- degrees

$\eta_t = \frac{q_t}{q}$ - Airplane tail coefficient

θ - Angle of pitch (angle between X axis and horizontal -- degrees)

λ - Root of stability quartic

$\mu = \frac{m}{\rho S c}$ - Relative airplane density factor (non-dimensional)

ρ - Mass density of air -- slugs/ft^3

$\tau = \frac{m}{\rho S V}$ - Time parameter -- seconds

ϕ - Phase angle -- degrees

ω - Angular frequency -- radians/sec

$\bar{\omega}$ - Angular frequency, radians per t/τ

A variable with subscript zero indicates the maximum value of that variable during an oscillation and may be either positive or negative.

Vertical bars indicate the conventional absolute value of any variable.

SIGN CONVENTION

Reference Axes

Normal stability axes (wind axes) are used.

X - axis - longitudinal axis - positive forward

Y - axis - lateral axis - positive along right wing

Z - axis - vertical axis - positive down

Linear Displacements

A linear displacement along a positive reference axis is considered positive.

Angular Displacements

An angular displacement which is clockwise when viewed from the origin looking along a positive reference axis is considered positive.

Velocities and Accelerations

Velocities and acceleration, either linear or angular, are considered positive in the same sense as the corresponding displacements.

Control Surface Deflections

Positive elevator angle is associated with a downward movement of the elevator trailing edge.

Phase Angles

A negative phase angle signifies a time lag of the response to the forcing function.

A positive phase angle signifies a time lead of the response to the forcing function.

ASSUMPTIONS

In the theoretical analysis and in the evaluation of the stability derivatives the following assumptions are made:

1. Stability axes (wind axes) are used.
2. The airplane is initially in level flight. (This means for stability axes $\cos\theta = 1$, $\sin\theta = \theta$)
3. All disturbances are small, so that the equations of motion may be considered linear.

4. The lift caused by the horizontal tail is negligible.
5. Small lateral disturbances which may exist do not affect the aerodynamic forces or pitching moments in the plane of symmetry.
6. Forces due to pitching velocities are negligible.
7. Change in pitching moment due to the rate of change of elevator angle is negligible.
8. Only longitudinal motion is considered. The moment of inertia is that about the Y axis.
9. Criteria for dynamic similarity were based on equal C_L of model and airplane (References 5 and 10).
10. Standard model flight conditions used in the solution of the equations of motion were:

$$V = 58.7 \text{ fps}$$

$$R = 37.5 \text{ ft}$$

at datum level = 4 ft. above the floor.

DESCRIPTION OF THE MODEL AND INSTRUMENTATION

The model used in this investigation was a one-tenth scale model of the Cessna 140 two-place light airplane. It was constructed by the authors. The construction consisted primarily of balsa-wood, paper-covered and doped; a construction similar to spin tunnel test models (Reference 9). Original intentions had been to make the model dynamically similar on the basis of equal lift coefficient (References 5 and 10). However, the choice of airplane and the scale used soon indicated that this would be physically impossible with available equipment, due to the low weight requirement and small size of the model. The choice of airplane was fixed by considerations previously mentioned, and scale was fixed by (1) budgetary reasons plus (2) the requirement of an indoor flying site to reduce stray wind disturbances on the model. It was decided to stay as close as possible to the weight limitation and measure the resulting moment of inertia of the model, using that and the actual weight in the non-dimensional equations of motion of the airplane of the harnessed model. This modification in no way affects the ability to judge the effectiveness of this type of flight as a test method.

The model was powered by a Bantam .19, cubic inch displacement, 1/10 HP (@ 9000 RPM), internal combustion, air-cooled, model airplane engine with glow ignition (Figure 1). This ignition saved weight by requiring no ignition components in the model; merely a $1\frac{1}{2}$-volt battery as a starting device. The engine was mounted inverted to preserve the contours of the upper cowling and it projected out of the lower cowling a short distance (Figure 2). A pressure type fuel feed system of commercial make was used

to prevent variation of engine speed due to change of fuel head in flight (Figure 1).

In order to give acess to the mechanism, engine and fuel system the wing, as well as various hatches were made removable (Figure 3 4).

In order to clarify the operation of the elevator pulsing mechanism it is necessary to describe the control of the model in flight. In normal flight the model flies in a circle around the operator on two wire lines which lead from a bellcrank (Figure 4) in the fuselage, through a guide near the wing tip to a handle in the hand of the operator. The model is flown with some yaw to the outside of the circle which is produced by offsetting the rudder and by attaching the bellcrank behind the C.G. The amount of this yaw is also controlled by adjusting the line guide on the wing. A push rod from the bellcrank links with the elevator horn so that a motion of the operator tending to increase tension in the top line from the handle and decrease tension in the bottom line is transmitted as an up deflection of the elevator.

The requirements on the elevator for the pulse input are that it (1) deflects from the trim elevator position, (2) returns to this position, and (3) remains locked during the ensuing transient motion. To this end a third wire from the operator to the model was employed. When a level equilibrium flight condition was attained, the operator transferred tension from the two flying wires to the third wire. The point of attachment of this wire was slightly aft of the model's C.G. in order to maintain slight outward yaw and hence line tension. The first result of tension on the third line was the application of a brake on the elevator push rod (Figure 4). This locked the elevator in the equilibrium position previously established. As

the tension was increased to counteract the full centrifugal force of the model, the third line also triggered a rubber-powered pulsing mechanism (Figure 4). The cam in this mechanism displaced the aft portion of the push rod, working against a spring which returned the elevator to the original locked position. The cam was cut to give a pulse of triangular shape with time, having a duration of approximately .04 seconds. By adjusting the position of the cam follower on the push rod, the amplitude of the pulse was varied. The cam contacting the follower closed an electrical circuit through a third wire which fired a flash bulb. After the elevator had been pulsed, the mechanism was automatically re-cocked for another run when the tension on the third line was released and the elevator again controlled by the operator.

Measurement of elevator angle was necessary in both phases of the testing. In the steady-state tests the angle required for equilibrium at each velocity had to be known, and in the dynamic tests the determination of the exact size of the pulse was necessary. This angle was to be measured with a Giannini Micro-torque. This instrument is an electrical potentiometer employing a rotating contact of very low mechanical torque gradient. Angular positions are measured electrically by suitable calibration. In this application the microtorque, acting as a variable resistance, was mounted in the fuselage and attached by a linkage to the elevator (Figure 4). Recording elevator position required two leads from the model to the center of the circle. Enameled steel flying wires were used for this purpose. From the operator's position the leads were continued to the recording apparatus on the ground (Figure 6). The steady-state elevator position was recorded by calibrating a voltmeter to elevator position. A recording oscillograph was

employed to record the pulse.

No in-flight measurements were possible in practice for two reasons. First, the vibration induced by the running engine was sufficient to destroy the electrical continuity of the micro-torque. Second, the friction introduced into the elevator system by the micro-torque linkage made control of the model marginal.

Weights adjustable fore and aft were used to alter the model C.G. position in running the steady-state phase. Normal C.G. for the model corresponded to normal C.G. for the full scale Cessna and was at 27.8% mac. This position was used for the dynamic phases.

Dynamic pitch-angle data was recorded by means of a motion picture camera tracking the model from the center of the circle. This camera was mounted on a heavy tripod equipped with leveling bolts and a revolving platen. A flash bulb in the 3rd line circuit, placed so that its flash would show on the film, was used to mark the instant of application of the pulse. The camera was equipped with a cross hair reticule. With the camera field vertical and the camera adjusted to track in the horizontal azimuth plane, these cross hairs were a reference for both pitch angle measurement and vertical displacement. The camera speed was calibrated for a time reference during the transient response.

The use of an armory was obtained for a testing site. This reduced the amount of stray air currents as compared with an outdoor site, and improved the chances of obtaining reproducible results.

TEST PROCEDURE

The C.G. location of the model was found by suspending it from three positions having wide angular separation about the pitch axis. The C.G. was at the intersection of plumb lines hung from the points of suspension.

The model's moment of inertia about the pitch axis was determined by swinging it as a compound pendulum. The method is described in Reference 6 and calculations given in Appendix G.

This C.G. location (27.8% mac) and moment of inertia (.012 slug ft^2) were used in calculating parameters for the equations of motion of the model.

Due to restrictions imposed by conditions at the flying site (low ceiling lamps) and by the light weight of the model, it was necessary to fly it from a 37.5 foot radius instead of the 50 foot radius originally contemplated. This resulted in a higher rate of yaw, but enabled the outward yaw angle of the model as set by the line guide on the wing, to be reduced because of the increase in centrifugal force with decrease in radius. The shorter radius was objectionable from the viewpoint of slipstream disturbances as the wake had less time to die out before being flown through again by the model.

A. Static Phase

No static-phase runs were made due to the above-mentioned mechanical difficulties. For the determination of the stick-fixed neutral point the model was to have been flown in steady level flight at a given C.G. position and velocity. The velocity would have been measured by timing a number of laps. The trim elevator position would have been measured with the calibrated voltmeter. A number of flights were to be made at this C.G. position with

various speeds. The speed would have been varied by a combination of engine adjustment and propeller change. This procedure of flying at various speeds was to be repeated for a number of C.G. locations.

B. Dynamic Phase

With the pulsing mechanism wound up, the model was flown level and the speed was measured. The electrical leads were connected to the operator's handle from the recording apparatus, and the recording oscillograph started. The camera was also started, and tracked the model under manual control. The pulse was triggered, the pitch angle data being recorded by the camera and the elevator pulse by the oscillograph. The record was continued until the stable transient died out.

RESULTS

No static phase data were possible because the micro-torque angle indicator would not record under the vibrating conditions produced by the engine of the model.

A total of fifteen flights were made during which the model was adjusted for controllable flight and qualitative data were observed for the dynamic phase. These consisted of approximate measurement of speed and visual observation of the following: characteristics of the phugoid mode, response to 5, 10, and 25-degree elevator pulses, and the behavior of the wake made visible by exhaust smoke.

All elevator-locked flights were above datum. Speeds observed were between 30-50 mph. The characteristics of the phugoid were erratic. Its period was observed to vary between 1.5-2.5 seconds. In some instances it was seen to diverge sharply. In one instance, during 40 seconds of

elevator-locked flight, several phugoid oscillations were seen to commence and damp out, under the influence of wake disturbances or other effects.

The 25-degree elevator pulse was found necessary for a visually observable pulse.

At the last pulse during one of the runs, the energy remaining in the mechanism was low enough to appreciably increase the duration of the pulse. The result was a greatly increased transient leading to a violent phugoid oscillation which almost terminated the entire experimental investigation.

DISCUSSION

Static Phase:

Various power settings are required during tests for elevator power and stick-fixed neutral point using harnessed flight. This results in changes in elevator power and the necessity for evaluating thrust outputs. Thus data reduction is complex, and since these characteristics may be found more easily from wind tunnel tests it was concluded that their calculation from harnessed flight tests is inadvisable. Another deterrant is external disturbance due to flight in the slipstream of the previous lap.

Dynamic Phase:

The initial intentions of this phase were to collect and analyze the flight data using the photographs of the time history of the pitch angle to plot $\frac{\theta}{\delta}$ against time. This plot was then to be graphically analyzed to find the frequency response as described in Reference 11. This experimentally determined frequency response curve was to be compared with the frequency response from the analysis of the transfer function of the equations of motion for the conditions of harnessed flight and of free flight. Since the equations of motion developed in Appendix A are non-dimensional and include the harnessing

forces as a separate term, they apply equally well to a model or to an airplane dynamically similar. Because the small size of the model prevented the attainment of a dynamically similar moment of inertia, the equations, as solved, refer not to the full scale Cessna 140 but to an airplane having all the Cessna longitudinal stability derivatives and characteristics (References 7 and 8) except for the mass and pitching moment of inertia. These two characteristics, found by direct measurement of the model and calculated, are those of an airplane dynamically similar to the model built for this investigation.

It was assumed from the information in the AMC report (Reference 5) that the stabilizing and damping effect of the harnessing line forces on the phugoid oscillation would eliminate this mode from any consideration in the analysis of flight data and would prevent it from becoming a problem in the testing technique. This did not prove to be the case. Although on flights with the elevators under control of the operator the model appeared stable with the C.G. at 27.8% mac; when the elevators were locked the model exhibited a very short period phugoid ($1\frac{1}{2}$ to $2\frac{1}{2}$ seconds period) when flown at elevations of about 10' above datum. Furthermore this phugoid oscillation was quite unstable, increasing to double amplitude in less than one period on numerous occasions. It was sufficiently unstable to make pulsing the elevator at the datum level (4' above the floor) when flying at 40 miles per hour possible only at the risk of destroying the model. It was decided that to enable data to be taken safely a higher datum plane was necessary, i.e., the operator standing on an elevated platform while flying the model. See sketch on page 19. Since the location permitting this was not available, no quantitative data were obtained at present writing. Instead, the emphasis

of the investigation was shifted to determination of the causes of the erroneous prediction and to analyzing methods which would make the fulfillment of the aims of the original investigation possible.

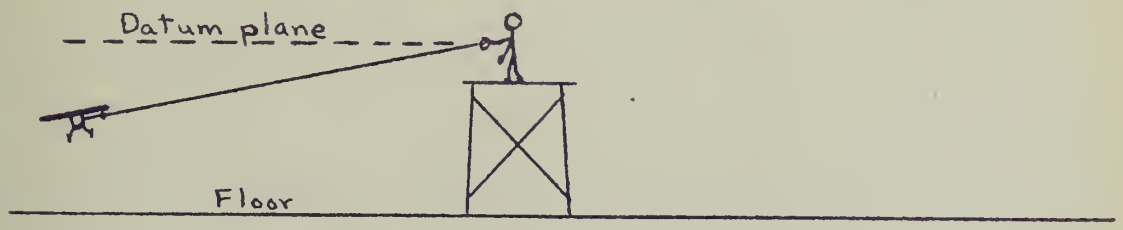

Sketch showing method of raising datum plane

In an attempt to find the causes for the discrepancy between the observed flights and the theory, the assumptions used in writing the equations of motion (Appendix A) were re-examined. It was confirmed that the angle of the lines leaving the model in the drag direction could be neglected. This angle was less than 2° under the most extreme flight conditions. It was also found that the angle in the gravity direction due to the weight of the lines was also negligible. Hence the assumption that the lines extend in a straight line from the operator to the model is valid even in so light a model. This is due primarily to the short radius employed. The conditions that the model must be charged with 3/4 of the drag of the harnessing wires and that the mass of the wires and their inertia effects upon non-steady motions can be neglected (due to the small mass of the wire) were also verified. Calculations supporting the preceding are shown in Appendix D.

However, observations showed that at the short radius flown (which was necessitated by indoor floor space and ceiling obstructions) and at the scale speed, the assumption that the circling flight would produce no aerodynamic effects on the longitudinal motion was not completely justified. Calculations show that the speed ratio between the velocity at the outer wing tip and the inner wing tip is 1.175 for the model used in this investigation. For comparison, to show that the short radius used here was no more detrimental to this condition than the radius used at the Wright Field testing facility, a calculation was made based upon their B-29 model (Reference 5). This resulted in a speed ratio of 1.22 between outer and inner wing tip. Therefore the model used in the present investigation was less affected by this variation of velocity with spanwise position than the large one flown at Wright Field on 150' lines. This speed ratio effect would produce a very complicated solution to the equations of motion. Therefore in the solution of the equations of motion it is omitted, with the reservation, however, that at least portions of the discrepancies between the theoretical solution for the frequency response and the experimental must be chargeable to this omission. An additional aerodynamic effect produced by the circling flight path is the interference effect of the model's own wake. Flight observations showed an intermittent disturbance which was most easily noticed by a sudden inward banking oscillation of the model. This was determined to occur when the model's outer wing passed through the slipstream remaining from a previous circuit. The banking oscillation was produced by the fact that in counterclockwise circling flight the outboard wing was being influenced by an upward component of both the slipstream and the inboard wing tip vortex. Confirmation of this reasoning was assisted

by the fact that the exhaust smoke of the engine made the slipstream wake visible. This wake was seen to leave the model approximately tangent to the flight circle with some downwash. See sketch below.

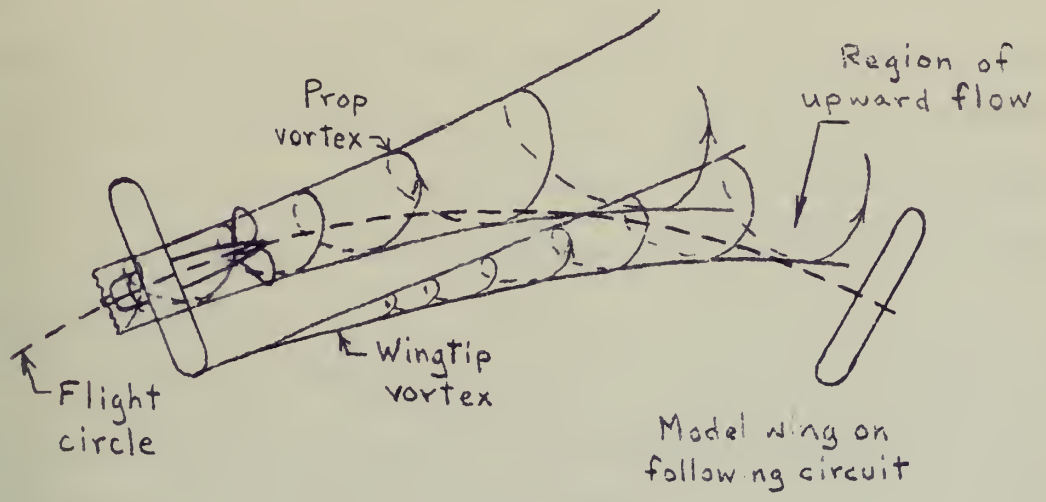

Sketch showing wake effects

Since, at scale speed the model passes the same azimuth point on the flight circle, and the wake appeared to widen as fast or faster than the curvature of the flight circle, the model crosses this turbulent area unless it is flown above the previous path by a reasonable distance.

All of the foregoing has not indicated any conclusive reason for the unstable phugoid which was observed. It was noted, however, that in both the analytical solution made by Braun in Reference 5 and in the initial solution for the present investigation, the familiar assumption of gliding flight condition, namely $C_T = 0$, was used. The solution obtained for this condition (Appendix C) using the equations developed for harnessed flight developed in Appendix A, gave as roots for the modes of motion:

$$\lambda_1 = -1.438, \quad \lambda_2 = -5.35$$

$$\lambda_{3,4} = -.001 \pm .263i$$

This indicates a very lightly damped, stable phugoid, with a period of 5.1 seconds which damps to 1/2 amplitude in 30 cycles. This, of course, was completely contrary to experimental observations. It is also of interest to note that the short period mode has degenerated into two real roots. This indicates that the model was overdamped, caused by too low a moment of inertia. This moment of inertia discrepancy had been expected. (See Description of Model).

In order to evaluate the effect of thrust on the equations, the characteristic equations, both with and without the harnessing force, were re-solved using the following thrust estimate: $C_T = C_D$ for all flight conditions close enough to the equilibrium condition such that the small angle approximations hold. This assumption makes $C_D^* = 0$ and $C_{D_\alpha}^* = 0$. Solution of the characteristic equation (Appendix C) yielded the following roots:

$$\lambda_1 = -1.705 \qquad \lambda_2 = -5.884$$

$$\lambda_{3,4} = .0055 \pm .265i$$

This solution indicates a trend in the right direction since it gives an unstable phugoid of essentially similar period to the glide condition (5.06 seconds), but which increases to double its amplitude in 5.32 cycles. This corroborates the observed instability of the phugoid although it does not show the rapid divergence which was observed in tests. It also shows that the power has only a very slight effect on the short period mode.

To check the validity of using the previous thrust assumption an additional solution was made of the characteristic equation (Appendix C) assuming that C_T was constant at the value of C_D at scale speed. This makes

$C_D^* = 0$ and $C_{D_\alpha}^* = C_{D_\alpha}$. The changes produced in the coefficients of the characteristic equation between this and the previous assumption were so small that they were within the accuracy of the calculation method used to factor the characteristic equation. It was therefore concluded that the previous assumption was sufficiently precise for the size of the factors and for the method used in extracting the roots.

As a further correlation of the period of the phugoid obtained from the equations with the period from observations the value of the period was corrected for flight at conditions other than at datum level. This was accomplished by the approximate relationship $\omega \cong \sqrt{\frac{C_L^2}{2}} = \frac{C_L}{\sqrt{2}}$ from Reference 1. Using the standard flight conditions and simple trigonometry, a force of -.119 lbs per foot of height from datum was calculated, (measuring directions and forces in airplane stability axes direction). This is converted into a C_L - correction factor by dividing by the weight and adding one: $C_{L_1} = C_L (1 + .078 h)$. Therefore denoting by subscript $(\ )_1$ conditions other than at datum, the following approximate relationship can be expressed:

$$\frac{P_1}{P} = \frac{\omega}{\omega_1} = \frac{C_L}{C_{L_1}} = \frac{C_L}{C_L(1+.078h)} = \frac{1}{1+.078h}$$

From the above it can be seen that flying the model at 13 feet above datum approximately halves the period. Therefore the observed results agree reasonably with the analysis insofar as the period of the phugoid is concerned. Also the quality of the stability of this mode is in agreement, namely they are both unstable. The only discrepancy is the rapidly divergent oscillation which was observed but which failed to materialize from the theory. This is unexplained.

The foregoing discussion has been primarily about the phugoid mode since this mode indicated the discrepancy in the initial assumptions upon which the equations of motion were solved. Now that reasonable agreement has been established between the theory and the qualitative observations, the assumptions which produced this agreement, namely $C_D^* = 0, C_{D_\alpha}^* = 0$, will be used in all further analysis. The phugoid mode is in itself of no interest in this investigation except as a complicating factor, since it is most markedly affected by the harnessing force of the lines (Appendix C). Examination of the short period roots, on the other hand, show practically no difference between those of harnessed and unharnessed flight. It is this fact that appears to make this testing method desirable for evaluation of dynamic stability above the frequency of the phugoid.

It is considered insufficient to compare the dynamics of complex systems on the basis of the characteristic equations alone. Such an analysis only considers the natural modes of motion of the system when disturbed, but not under the action of a forcing function. Since the normal dynamic testing methods involve the application of a forcing function, it is more reasonable to compare harnessed and free flight on the basis of the frequency response. This frequency response can be obtained in the conventional manner by solving the transformed equations of motion for the transfer function $\frac{\theta}{\delta}$ as shown in Appendix B. The transfer functions to a step input were reduced to the frequency domain by the graphical logarithmic method of Reference 2, and illustrated in Appendix E. The frequency response, as obtained from the analysis of the equations of motion for both harnessed and unharnessed flight are plotted on Figures 7 and 8 . These are the curves with which the experimental frequency response was to have been compared.

Examination of the frequency response curves Figures 7 and 8 show that above a frequency of 1.0 radian per $^{*}/_{T}$ the frequency response for harnessed flight is identical in shape with that of the free flight, but the amplitude of the former is less. The fact that this difference in amplitude is a constant factor is quite evident from the logarithmic plot of Figure 10 . On this plot there is a constant 2 decibel gain difference. Converting this gain difference into amplitude it was determined that the amplitude of the harnessed model was 80% of the correct free flight value at all frequencies above $\bar{\omega} = 1.0$. This loss of amplitude is not unreasonable since the lines offer restraining forces which would tend to limit the amplitude of oscillation in response to a forcing function.

Since the aforementioned loss in amplitude is tied up in numerous terms of the transfer function, it would be difficult to evaluate it directly from the harnessing force. However, it would appear that the change in amplitude is a function only of the mass, speed, and flying radius of the model. Therefore it should be possible to evaluate this percentage change for a variety of permutations of these items and tabulate the result to be used in adjusting experimentally determined frequency response curves to free flight.

In order to see if the transfer function of the harnessed flight $\frac{\theta}{\delta}$ gave a transient response which was similar, qualitatively, to that observed when the model elevator was pulsed; and also to establish desirable frame speed for the recording camera, it was considered necessary to solve for the transient response. In order to simplify this calculation, a square pulse was assumed instead of the triangular one actually imposed on the model. It should be noted that a triangular pulse was chosen for the model to enable the simplified method of Reference 11 to be used in converting from the experimental transient response back to the frequency response.

The mechanical details of determining the transient response from the transfer function are covered in the literature. Numerous methods may be used. The one chosen for use here is the Heaviside expansion which is described in References 1 and 4, namely,

Given the transfer function $\frac{\theta}{\delta}(\lambda) = \frac{F(\lambda)}{G(\lambda)}$

and roots of $G(\lambda)$ are $\lambda_1, \lambda_2, \lambda_3 \cdots \lambda_n$ none of which are zero or repeated roots,

Then $\frac{\theta}{\delta}(t) = \frac{F(0)}{G(0)} + \sum_{i=1}^{n} \frac{F(\lambda_i)}{\lambda_i G'(\lambda_i)}$ where $G'(\lambda_i) = \frac{d\,G(\lambda)}{d\lambda}$

This solution is the time response to a unit step input (Appendix E). By using the method of Reference 4 the response to a pulse of finite width can be found. This method considers the pulse as being made up of a positive unit step followed at time Δt by a negative unit step. By superposing these two inputs a unit pulse of width Δt is obtained. By the principle of the Convolution Theorem the output is then the result of superposing the outputs to these step inputs. These outputs are identical in shape but of opposite sign and separated in time by an interval Δt. These operations were accomplished on logarithmic coordinates and the results are plotted on Figures 11 and 12. These are time histories of the pitch angle θ per unit elevator input. The solutions are for a pulse of .04 seconds, .10 seconds, and .14 seconds. They show that the pitch changes of the transient are of reasonable amplitude for these two pulse widths, provided that large elevator deflections are used. This corroborates the visually observed effects. They also show that the pulse must be kept short or the transient response due to the short period mode is negligible compared to the phugoid.

If a camera record at 100 frames per second were made, the pictures at each 1/100th of a second would give ample data from which to plot an experimental curve similar to Figure 12. Also, since the slower decaying of the two short period roots was reduced to 1½% of its initial value at .7 seconds, only the first 7/10ths of a second would be used in the graphical analysis (Reference 11) to obtain the frequency response of frequencies associated with the short period mode.

CONCLUSIONS

The use of harnessed models in circling flight for evaluating longitudinal stability of full-scale airplanes has been investigated qualitatively.

It was determined that this method is inadvisable for finding elevator power and stick-fixed neutral point because of the variations required in test power settings and because of continuous slipstream disturbance.

The method appeared favorable for obtaining transient pitch-angle response to a pulse elevator input, employing a high-speed motion-picture camera to record transients.

There is a definite lower limit on the size of models which can be used in this method, considering dynamic similarity, due to the critical weight requirement and the necessary mechanical installations.

The use of an indoor flying site featuring a raised platform for the operator is recommended. This would permit initiation of transients at the datum plane of $\Delta\phi = 0$ (flying wires horizontal) and would prevent destruction of the model in the event of ensuing unstable phugoid oscillations.

Previous to recording data the model should be flown below datum. To preclude effects of wake disturbance, data would have to be recorded within one lap of datum-level flight.

If further investigation of this technique is intended with the Cessna configuration, it is recommended that a model of at least twice the size, i.e., one-fifth scale, be used.

REFERENCES

1. Perkins, C. D. and Hage, R. E., AIRPLANE PERFORMANCE, STABILITY AND CONTROL, John Wiley, Second Printing, 1950.
2. Brown, G. S. and Campbell, D. P., PRINCIPLES OF SERVOMECHANISMS, John Wiley, Third Printing, corrected, 1950.
3. Pipes, L. A., APPLIED MATHEMATICS FOR ENGINEERS AND PHYSICISTS, McGraw-Hill, 1946.
4. Nikolsky, A. A., HELICOPTER ANALYSIS, John Wiley, 1951.
5. Air Force Technical Report No. 5979, TESTING LONGITUDINAL STABILITY OF MODELS IN HARNESSED CIRCLING FLIGHT.
6. National Advisory Committee for Aeronautics, Technical Note No. 1629, THE EXPERIMENTAL DETERMINATION OF THE MOMENTS OF INERTIA OF AIRPLANES BY A SIMPLIFIED COMPOUND-PENDULUM METHOD.
7. Princeton University Aeronautical Engineering Laboratory Report No. 160, DETERMINATION OF THE ELEVATOR POWER AND THE DAMPING IN PITCH OF THE CESSNA 140 AIRPLANE FROM FLIGHT TESTS.
8. Princeton University Aeronautical Engineering Laboratory Report No. 173, CORRELATION OF PERFORMANCE DATA ON THE CESSNA 140 AIRPLANE.
9. National Advisory Committee for Aeronautics, Technical Report No. 557, PRELIMINARY TESTS IN THE NACA FREE-SPINNING WIND TUNNEL.
10. National Advisory Committee for Aeronautics, Technical Note No. 268, MASS DISTRIBUTION AND PERFORMANCE OF FREE FLIGHT MODELS.
11. Journal of the Aeronautical Sciences, January 1950, THE PULSE METHOD FOR THE DETERMINATION OF AIRCRAFT DYNAMIC PERFORMANCE.

APPENDIX A

Development of general equations of motion to include harnessing forces. This development is essentially similar to that of Reference 5, and uses the same assumptions.

Assumptions are as follows.

(1) The lines extend in a straight line from the operator to the model.

(2) The height at which the model flies to maintain the harnessing lines in the horizontal plane is referred to as datum height and the model flying at this height is flying in the datum plane. In this plane the wings of the model are assumed level.

(3) The bank angle of the model ($\Delta\phi$) because of the action of the harnessing wire guide on the inboard wing tip equals the angle the lines make with the horizontal.

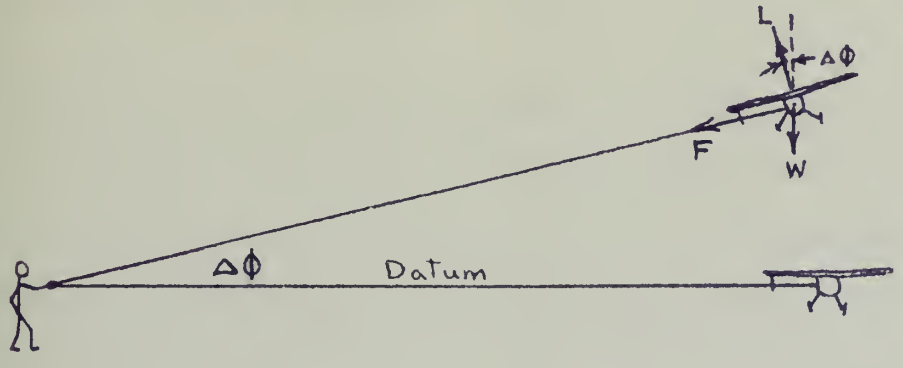

(4) For small displacements of the model from datum, $\sin\Delta\phi = \Delta\phi$, $\cos\Delta\phi = 1$, and F remains constant.

(5) The equations of motion use stability (wind) axes.

(6) Aerodynamic effects due to curvature of the flight path are neglected.

The equations of longitudinal motion are as follows:

$$\Sigma F_x = m\dot{V} = -C_D \tfrac{1}{2}\rho V^2 S - W\sin\gamma + C_T \tfrac{1}{2}\rho V^2 S \qquad (1\text{-a})$$

$$\Sigma F_z = -mV\dot{\gamma} = -C_L \tfrac{1}{2}\rho V^2 S + W\cos\gamma + \frac{mV^2}{R}\sin\Delta\phi \qquad (1\text{-b})$$

$$\Sigma M_Y = I_Y(\ddot{\alpha} + \ddot{\gamma}) = C_m \tfrac{1}{2}\rho V^2 S c \qquad (1\text{-c})$$

These equations are then linearized in the usual fashion by considering each term: $F(V, \gamma, \alpha, \phi, \cdots) = \frac{\partial F}{\partial V}\Delta V + \frac{\partial F}{\partial \alpha}\Delta\alpha + \frac{\partial F}{\partial \gamma}\Delta\gamma + \frac{\partial F}{\partial \Delta\phi}\Delta(\Delta\phi) + \cdots$

After letting $C_D^* = C_D - C_T$ this results in

$$m\dot{V} + (C_D^*\rho S V)\Delta V + (C_{D_\alpha}^* \tfrac{1}{2}\rho V^2 S + W)\Delta\alpha + W\Delta\gamma = 0 \qquad (2\text{-a})$$

$$mV\dot{\gamma} - (C_L\rho V S - 2\frac{mV}{R}\Delta\phi)\Delta V - (C_{L_\alpha} \tfrac{1}{2}\rho V^2 S)\Delta\alpha - W\sin\gamma\,\Delta\gamma + \frac{mV^2}{R}\Delta\phi = 0 \qquad (2\text{-b})$$

$$I_Y(\ddot{\alpha} + \ddot{\gamma}) - C_{m_V} \tfrac{1}{2}\rho V^2 S c\,\Delta V - C_{m_\alpha} \tfrac{1}{2}\rho V^2 S c\,\Delta\alpha - C_{m_{\dot{\alpha}}} \tfrac{1}{2}\rho V^2 S c\,\Delta\dot{\alpha} - C_{m_\theta} \tfrac{1}{2}\rho V^2 S c\,\Delta\dot{\theta} - C_{m_{\delta_e}} \tfrac{1}{2}\rho V^2 S c\,\Delta\delta_e = 0 \qquad (2\text{-c})$$

In order to put the term $\Delta\phi$ in terms of the longitudinal variables, substitute $\Delta\phi = \frac{h}{R}$ (where h is the vertical distance from datum), and differentiate with respect to time. Neglecting higher-order terms this gives:

$$mV\dot{\gamma} - W\sin\gamma\,\Delta\dot{\gamma} - C_L\rho V S\,\Delta\dot{V} - C_{L_\alpha} q_0 S\,\Delta\dot{\alpha} + \frac{F}{R}\frac{dh}{dt} = 0 \qquad (2\text{-b})_1$$

$$dh/dt = V\sin\gamma \quad \text{where } \gamma = \gamma_0 + \Delta\gamma$$

However, since initial conditions specify level flight at datum level, $\gamma_0 = 0$, and $\therefore \frac{dh}{dt} = \Delta\gamma$, and from equation (1-a), $-W\sin\Delta\phi = C_D^* q_0 S$, therefore equation $(2\text{-b})_1$ becomes

$$mV\dot{\gamma} + C_D^* q_0 S\,\Delta\gamma - C_L\rho V S\,\Delta\dot{V} - C_{L_\alpha} q_0 S\,\Delta\dot{\alpha} + \frac{FV}{R}\Delta\gamma = 0$$

Dividing through equation a and b by $\frac{1}{2}\rho V^2 S = q_0 S$ and equation c by $\frac{1}{2}\rho V^2 S_c = q_0 S_c$ and making substitutions as follows:

$$\mu = \frac{\Delta V}{V} \qquad f = \frac{F}{R}\frac{\tau}{\rho V S}$$

$$\dot{\mu} = \frac{\dot{V}}{V} \qquad h = \frac{2}{\mu}\left(\frac{k_Y}{c}\right)^2$$

$$\tau = \frac{m}{\rho S V} \qquad k_Y^2 = \frac{I_Y}{m}$$

$$\mu = \frac{m}{\rho S c}$$

and using the operator d to indicate differentiation with respect to t/τ, and considering all α, γ as being the displacements from initial conditions (i.e., $\Delta\alpha, \Delta\gamma$) gives the linearized non-dimensional form of the equation: These are expressed in operator form.

$$\left(d + C_D^* + \tfrac{1}{2}C_{D_\mu}^*\right)\mu + \tfrac{1}{2}C_{D_\alpha}^*\alpha + \tfrac{1}{2}C_L\gamma = 0 \tag{3-a}$$

$$C_L d\mu + \tfrac{1}{2}C_{L_\alpha} d\alpha - \left(d^2 + \tfrac{1}{2}C_D^* d + f\right)\gamma = 0 \tag{3-b}$$

$$-\tfrac{1}{h}C_{m_\mu} d\mu + \left[d^2 - \left(\frac{C_{m_{d\theta}} + C_{m_{d\alpha}}}{h}\right)d - \tfrac{1}{h}C_{m_\alpha}\right]\alpha + \left(d^2 - \frac{C_{m_{d\theta}}}{h} d\right)\gamma = \tfrac{1}{h}C_{m_{\delta_e}}\delta_e\left(t/\tau\right) \tag{3-c}$$

In the analysis following, $C_{D_\mu}^*$ and C_{m_μ} will be considered small and neglected.

APPENDIX B

Development of characteristic equation and transfer function $\frac{\theta}{\delta_e}$.

Solution to the equations of motion (Equations 3, Appendix A) is made by assuming a solution of form

$$u = u_1 e^{\lambda t/\tau}, \quad \alpha = \alpha_1 e^{\lambda t/\tau}, \quad \theta = \theta_1 e^{\lambda t/\tau}$$

with the $\frac{1}{h} C_{m_\delta} \delta_e = 0$ for the stick-fixed condition with δ_e measured from equilibrium elevator position.

This results in

$$(C_D^* + \lambda)u_1 + \tfrac{1}{2}(C_{D\alpha} - C_L)\alpha_1 + \tfrac{1}{2} C_L \theta_1 = 0 \qquad (4\text{-a})$$

$$C_L \lambda u_1 + \left[\lambda^2 + \left(\frac{C_D^* + C_{L\alpha}}{2}\right)\lambda + f\right]\alpha_1 - \left[\lambda^2 + \frac{C_D^*}{2}\lambda + f\right]\theta_1 = 0 \qquad (4\text{-b})$$

$$\left[\frac{C_{m_{d\alpha}}}{h}\lambda + \frac{C_{m_\alpha}}{h}\right]\alpha_1 + \left[\frac{C_{m_{d\theta}}}{h}\lambda - \lambda^2\right]\theta_1 = 0 \qquad (4\text{-c})$$

For these homogeneous algebraic equations to have other than a trivial solution the determinants of their coefficients must vanish.

Expansion of this 3rd-order determinant gives an equation of the form

$$b_5\lambda^5 + b_4\lambda^4 + b_3\lambda^3 + b_2\lambda^2 + b_1\lambda + b_0 = 0 \qquad (5)$$

By defining the combination $\frac{C_{m_{d\theta}} + C_{m_{d\alpha}}}{h} = M$ and $C_L^2 + C_D^{*2} = C_R^2$, the coefficients of the characteristic equation above are expressed as

$$b_5 = -1$$

$$b_4 = M - \tfrac{3}{2} C_D^* - C_{L\alpha}$$

$$b_3 = \tfrac{3}{2} C_D^* M - \frac{C_R^2}{2} + \frac{C_{L\alpha}}{2}\left(C_{m_{d\theta}} - C_D^*\right) + \frac{C_{m_\alpha}}{h} + \frac{C_L}{2} C_{D_\alpha}^* - f$$

$$b_2 = \frac{C_R^2}{2} M - \frac{C_L}{2} C_{D_\alpha}^* \frac{C_{m_{d\theta}}}{h} + \frac{3}{2} C_D^* \frac{C_{m_\alpha}}{h} + f(M - C_D^*) + \frac{C_D^*}{2} C_{L\alpha} \frac{C_{m_{d\theta}}}{h}$$

$$b_1 = \frac{C_R^2}{2}\frac{C_{m_\alpha}}{h} + f\left(\frac{C_{m_\alpha}}{h} + M C_D^*\right)$$

$$b_0 = f \frac{C_{m_\alpha}}{h} C_D^*$$

Solution for the transfer function $\frac{\theta}{\delta_e}$ to a step input is made by using the Laplace transform on the equations of motion (Equations 4). Since all initial conditions are assumed zero for the variables used, and the transform of a step function is unity in the Laplace transform as defined in Reference 3, this results in equations 6 below.

$$(C_D^* + \lambda)\mu + \tfrac{1}{2}(C_{D\alpha} - C_L)\alpha + \tfrac{1}{2}C_L\theta = 0 \qquad (6\text{-a})$$

$$C_L\lambda\mu + \left[\lambda^2 + \left(\frac{C_D^* + C_{L\alpha}}{2}\right)\lambda + f\right]\alpha - \left[\lambda^2 + \frac{C_D^*}{2}\lambda + f\right]\theta = 0 \qquad (6\text{-b})$$

$$\left[\frac{C_{m_{\dot\alpha}}}{h}\lambda + \frac{C_{m_\alpha}}{h}\right]\alpha + \left[\frac{C_{m_{\dot\theta}}}{h}\lambda - \lambda^2\right]\theta = -\frac{1}{h}C_{m_\delta}\delta_e \qquad (6\text{-c})$$

Note: Although the left sides of the equations above appear similar to equations 4, in equations 6, $\mu, \alpha,$ and θ are variables of t/τ, while in equations 4, $\mu_1, \alpha_1,$ and θ_1 are constants. Solving equations 6 by determinants for $\frac{\theta}{\delta_e}$ gives a solution of the form:

$$\frac{\theta}{\delta_e}(\lambda) = \frac{a_3\lambda^3 + a_2\lambda^2 + a_1\lambda + a_0}{b_5\lambda^5 + b_4\lambda^4 + b_3\lambda^3 + b_2\lambda^2 + b_1\lambda + b_0} \qquad (7)$$

Where the b coefficients of the denominator are those of the characteristic equation and

$$a_3 = 1$$

$$a_2 = \tfrac{1}{2}(3C_D^* + C_{L\alpha})$$

$$a_1 = \tfrac{1}{2}\left[C_R^2 + C_D^* C_{L\alpha} - C_L C_{D\alpha}^*\right] + f$$

$$a_0 = C_D^* f$$

APPENDIX C

Since the characteristic equation is the denominator of the transfer function $\frac{\theta}{\delta}(\lambda)$, all solutions will be made for the transfer function only.

All solutions will be based upon the following so-called standard flight conditions (all angles in radians):

V = 58.7 ft/sec (40 mph)

C_L = .232 from $\frac{W}{q_0 S}$

C_D = .0616 from wind tunnel polar (Reference 8) corrected by addition of wire drag (Appendix D)

W = 1.53 lb	R = 37.5 ft	μ = 25.6
S = 1.59 ft^2	τ = .214	h = .0843
b = 3.28 ft	f = .119	m = .0476 slug ft^2
AR = 6.76	ρ = .00238	C_{m_α} = -.406 from Reference 8
C = .492 ft	C_{L_α} = 4.62	e = .869 from Reference 8

$$C_{D_\alpha} = \frac{2C_L}{e\pi AR} = .116$$

The following various thrust conditions were considered using harnessed flight equations:

Condition I - $C_T = 0$ constant

Condition II - $C_T = C_D$ at all α and μ $(C_{D_\alpha}^* = 0)$

Condition III - $C_T = C_D$ at equilibrium α and μ, and is constant at that value $(C_{D_\alpha}^* = C_{D_\alpha})$.

These conditions produce the following changes in the components of a_i and b_i :

	Condition I	Condition II	Condition III
η_t	1.0	1.28	1.28
C_D^*	.0616	0	0
$C_{D_\alpha}^*$	.116	0	.116
$\frac{C_R^2}{2}$	.0277	.0269	.0269

The following terms depend upon tail efficiency η_t. The Condition values were obtained from References 7 and 8 and corrected for η_t.

C_{m_δ}	-.751	-.964	-.964
$C_{m_{d\theta}}$	-.149	-.190	-.190
$C_{m_{d\alpha}}$	-.0465	-.0594	-.0594

Solution of the transfer functions for harnessed flight gave

Condition I: $\frac{\theta}{\delta}(\lambda) = \frac{-8.91\ (\lambda^3 + 2.37\lambda^2 + .252\lambda + .005)}{(\lambda^5 + 6.99\lambda^4 + 8.249\lambda^3 + .7559\lambda^2 + .5655\lambda + .018)}$

Condition II: $\frac{\theta}{\delta}(\lambda) = \frac{-11.43\ (\lambda^2 + 2.31\lambda + .1437)}{(\lambda^4 + 7.577\lambda^3 + 10.165\lambda^2 + .4125\lambda + .702)}$

Condition III: $\frac{\theta}{\delta}(\lambda) = \frac{-11.43\ (\lambda^2 + 2.31\lambda + .1417)}{(\lambda^4 + 7.577\lambda^3 + 10.152\lambda^2 + .3823\lambda + .702)}$

Factored forms of the preceding are:

Condition I: $\frac{\theta}{\delta}(\lambda) = \frac{-8.91\ (\lambda + .0262)(\lambda + .084)(\lambda + 2.256)}{(\lambda + .0327)(\lambda + 1.438)(\lambda + 5.53)(\lambda^2 + .002\lambda + .2627^2)}$

Condition II: $\frac{\theta}{\delta}(\lambda) = \frac{-11.43\ (\lambda + .065)(\lambda + 2.245)}{(\lambda + 1.705)(\lambda + 5.884)(\lambda^2 - .012\lambda + .2642)}$

Condition III: $\frac{\theta}{\delta}(\lambda)$ = Same as Condition II

Condition II was established as the most proper condition and the transfer function was re-solved for unharnessed flight by computing the coefficients for $f = 0$.

Condition II+- Free flight:

$$\frac{\theta}{\delta}(\lambda) = \frac{-11.43\,(\lambda + .012)(\lambda + 2.298)}{(\lambda + 1.704)(\lambda + 5.875)(\lambda^2 - .0018\lambda + .113^2)}$$

APPENDIX D

Calculation of drag effects upon the harnessing wires. This solution assumes no outward yaw of the model. Axes are as shown.

T - line tension = F = $\frac{mV^2}{R}$

C_D = 1.2 two-dimensional flow C_D of cylinder at low N_R based on frontal area.

S_w = area per foot of wire normal to velocity

= .0007 for .008" wire

= .001 for .012" wire

$q_b = 1/2\rho v^2$ where v is velocity of wire at station x

$v = \frac{V}{R}x$

$\therefore q_b = 1/2\,\rho\left(\frac{V}{R}\right)^2 x^2$

$dD = C_D S_q dx = Kx^2 dx$

Consider an element of wire, length dx, loaded by the drag Kx^2dx.

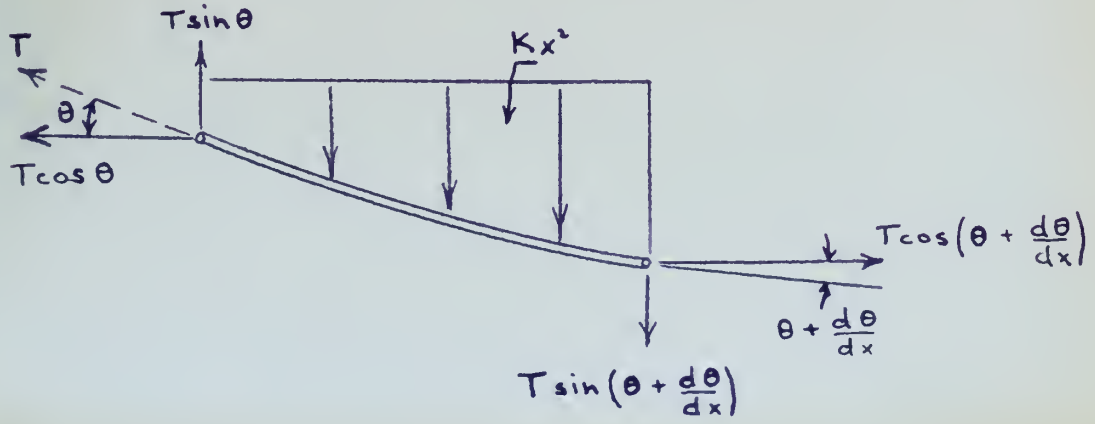

Taking the summation of forces in the drag direction, assuming T remains constant over the element,

$$\Sigma F_Y = T\sin\theta - Kx^2 - T\sin\left(\theta + \frac{d\theta}{dx}\right) = 0$$

$$T\sin\theta - Kx^2 - T\sin\theta\cos\frac{d\theta}{dx} - T\cos\theta\sin\frac{d\theta}{dx} = 0$$

$$\cos\theta \cong 1, \quad \cos\frac{d\theta}{dx} \cong 1, \quad \sin\frac{d\theta}{dx} = \frac{d\theta}{dx} = \frac{d^2y}{dx^2}$$

therefore $$Kx^2 - T\frac{d^2y}{dx^2} = 0$$

Integrating gives

$$\frac{dy}{dx} = -\frac{Kx^3}{3T} + C$$

Integrating again gives

$$y = -\frac{Kx^4}{12T} + Cx + D$$

Solving by constants for end conditions:

$$D = 0$$

$$C = \frac{Kl^3}{12T}$$

Therefore

$$\theta\Big]_{x=0} = \frac{Kl^3}{12T}$$

$$\theta\Big]_{x=l} = -3\theta\Big]_{x=0}$$

$$K = \rho\frac{C_D}{2}\left(\frac{V}{R}\right)^2 S = \frac{35}{10^4}S$$

$$\theta\Big]_{x=l} = -\frac{\rho C_D R^2 S}{8m} = -13.72\,S$$

For tension shared by all wires equally (most conservative condition)

$$\theta_{x=l} = (-13.72)(.00234)\,57.3 = 1.84^\circ$$

Drag of wires:

$$D = \int_{2.5}^{37.5} dD\,dx = K\int_{2.5}^{37.5} x^3 dx$$

$$D_{w_1} = \frac{35(.001)}{10^4}\left[x^3/3\right]_{2.5}^{37.5} = .0619 \text{ lb for .012" wire}$$

$$D_{TOTAL} = D_{w_1} + 2D_{w_2} = D_{w_1} + (2)\frac{2}{3}D_{w_1}$$

$$= \left(\frac{7}{3}\right)D_{w_1} = .144 \text{ lb.}$$

Determination of proportion of wire drag adding to airplane drag:

Centroid of wire drag:

$$\bar{X}_D = \frac{1}{D}\int_{l_1}^{l_2} dD_x\,dx = \frac{1}{D}\int_{l_1}^{l_2} K x^3 dx$$

$$= \frac{1}{D}\int_{2.5}^{37.5} K x^3 dx = \frac{K}{D}\left[\frac{x^4}{4}\right]_{2.5}^{37.5}$$

$$\text{but } D = K\frac{x^3}{3}\Big]_{2.5}^{37.5}$$

Therefore

$$\bar{X}_D = \frac{K\frac{x^4}{4}}{K\frac{x^3}{3}}\Bigg|_{2.5}^{37.5} = \frac{3}{4}x\Big|_{2.5}^{37.5}$$

Therefore the wire drag centroid is located 3/4 of the distance along the radius from the operator.

D wires = 3/4 (.144) = .108#

Converting to conventional coefficient:

$$C_{D_w} = \frac{.108}{6.52} = .0166$$

Total model drag coefficient:

$$C_D = C_{D_{MODEL}} + C_{D_{INTERFERENCE}} + C_{D_{WIRE}}$$

$$= .040 + .005 + .0166 = .0616$$

Total drag:

$$D = C_D q_0 S = .0616(6.52) = .402^{\#}$$

Calculation of Line Tension:

Centrifugal Line Force $T_1 = \frac{mV^2}{r} = \frac{W}{g}\frac{V^2}{r}$

$= \frac{.0476}{37.5} \cdot (58.7)^2 = 4.38$ lbs

Side Force @ 5° of $\beta = C_y = C_{y_\beta}\beta = .008 \times 5 = .040$

$Y_1 = C_{y_\beta} S = (.040)6.52 = .26$ lbs

Total Line Tension = 4.64 lbs.

APPENDIX E

Frequency response calculation of model in harnessed flight, $C_T = C_D$:

$$\frac{\theta}{\delta}(j\omega) = \frac{-2.37\left(1+\frac{j\omega}{.065}\right)\left(1+\frac{j\omega}{2.245}\right)}{\left(1+\frac{j\omega}{5.884}\right)\left(1+\frac{j\omega}{1.705}\right)\left[\left(\frac{j\omega}{.2647}\right)^2 - .167 j\omega + 1\right]} \quad \bigstar$$

Components of the Lm-Ang plot are given Figure 9 and are added to obtain the complete frequency response in Figure 10. This result is replotted on cartesian coordinates in Figures 7 and 8 .

★ $K = 2.37$

$20\log_{10} 2.37 = 7.5\,db$

$$\text{Lm}\,\frac{\theta}{\delta}(j\omega) = 20\log_{10}2.37 + 20\log_{10}\sqrt{1+\left(\frac{j\omega}{.065}\right)^2} + 20\log_{10}\sqrt{1+\left(\frac{j\omega}{2.245}\right)^2}$$

$$- 20\log_{10}\sqrt{1+\left(\frac{j\omega}{5.884}\right)^2} - 20\log_{10}\sqrt{1+\left(\frac{j\omega}{1.705}\right)^2} - 20\log_{10}\sqrt{\left[1+\left(\frac{j\omega}{.2647}\right)^2\right]^2+(.167j\omega)^2}$$

$$\phi \text{ of } \frac{\theta}{\delta}(j\omega) = \tan^{-1}\frac{\omega}{.065} + \tan^{-1}\frac{\omega}{2.245} - \tan^{-1}\frac{\omega}{5.884}$$

$$- \tan^{-1}\frac{\omega}{1.705} - \tan^{-1}\frac{(-.167\omega)}{1+\left(\frac{j\omega}{.2647}\right)^2}$$

APPENDIX F

Transient response by Heaviside method:

$$\frac{\theta}{\delta}(t) = \frac{P(0)}{Q(0)} + \sum_{n=1}^{m} \frac{P(\lambda_n) e^{\lambda_n t}}{\lambda_n Q'(\lambda_n)}$$

Harnessed flight, $C_T = C_D$:

$$\frac{\theta}{\delta} = \frac{-11.43[\lambda^2 + 2.31\lambda + .1459]}{[\lambda^4 + 7.577\lambda^3 + 10.165\lambda^2 + .4125\lambda + .702]}$$

$$\frac{P(0)}{Q(0)} = \frac{-11.43(.1459)}{.702} = -2.376$$

$\lambda_1 = -1.075$:

$$P(\lambda_1) = 2.907 - 3.939 + .1459$$
$$= -.886$$

$$Q'(\lambda_1) = 4\lambda_1^3 + 3(7.577)\lambda_1^2 + 2(10.165)\lambda_1 + .4125$$
$$= -19.82 + 66.079 - 34.66 + .4125$$
$$= 12.01$$

$$\frac{KP(\lambda_1)}{\lambda_1 Q'(\lambda_1)} = \frac{.886(11.43)}{-1.075(12.01)} = -.7844$$

$\lambda_2 = -5.885$:

$$P(\lambda_2) = 34.62 - 13.592 + .1459$$
$$= 21.174$$

$$Q'(\lambda_2) = -814.8 + 786.95 - 119.96 + .4125$$
$$= -147.40$$

$$\frac{KP(\lambda_2)}{\lambda_2 Q'(\lambda_2)} = \frac{-11.43(21.174)}{-5.884(147.40)} = .2790$$

$$\frac{\theta}{\delta}(t) = -2.376 - .7844e^{-1.075t/\tau} + .2790e^{-5.884t/\tau}$$

(Short period mode only)

Long period mode of harnessed flight, $C_T = C_D$:

$$\frac{\theta}{\delta}(t) = 4.12e^{.027t}\sin(71t + 135.5^\circ)$$

The complete solution for this condition is plotted in Figure 12.

Short period transient, free flight, $C_T = C_D$:

$$\frac{\theta}{\delta}(t) = -2.383 - .559e^{-1.704t/4} - .2826e^{-5.875t/4}$$

APPENDIX G

Sample calculation of Moment of Inertia I_Y

$$I_Y = \frac{(Wl + \omega l')T^2}{4\pi^2} - \left(\frac{W}{g} + V\rho\right)l^2 - I_G$$

W = Model weight = 1.53 lb.

l = Pendulum length = 1.23 ft.

ω = Swinging gear weight = .0331 lb.

l' = Swinging gear pendulum length = 1.053 ft.

T = Measured period of oscillation = 1.335 sec.

V = Model volume = .216 ft.^{3}

ρ = Air density = .00238 slugs/ft.^{3}

g = Gravitational acceleration = 32.2 $\frac{\text{ft}}{\text{sec.}^2}$

I_G = Inertia of swinging gear

$= \frac{\omega l' t^2}{4\pi^2} = .000975$

where t = measured period of oscillation of the gear alone = 1.31 sec.

Substituting in the above equation for I_Y :

$$I_Y = .0124 \text{ slug ft.}^2$$

Figure C

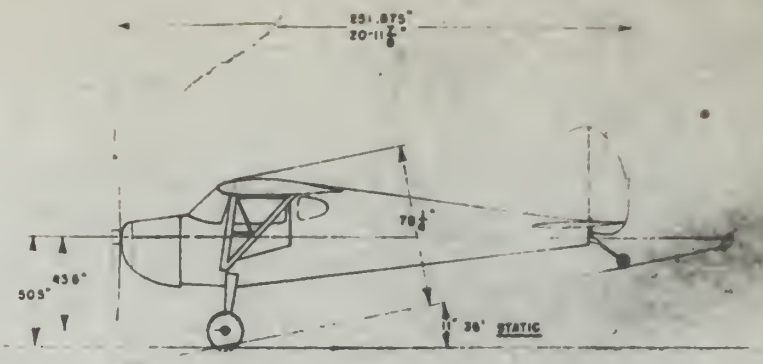

AREAS —

WING (INC FUSELAGE)	159.29	SQ. FT
STABILIZER	14.64	"
FIN	6.468	"
ELEVATOR (PLUS TAB)	9.88	"
RUDDER	5.752	"
AILERON (TOTAL)	14.08	"
FLAPS	8.736	"
ELEVATOR TAB	6.92	"

ANGLES —

INCIDENCE STABILIZER	-2 1/2°
INCIDENCE WING	+1°
DIHEDRAL	+1°
RUDDER TRAVEL	± 16° ±1°
ELEVATOR TRAVEL	± 20° ±1°
AILERON TRAVEL	↑ 22° ±1°
	↓ 14° ±1°
FLAP TRAVEL	- 40° ±2°
ELEVATOR TAB	+ 6° ±1°
	- 33° ±1°

ENGINE — CONTINENTAL

MODEL	C 85
H.P.	85
R.P.M.	2875

PROP. DIA. 76" (MAX.)

WEIGHTS

EMPTY	874
GROSS	1450

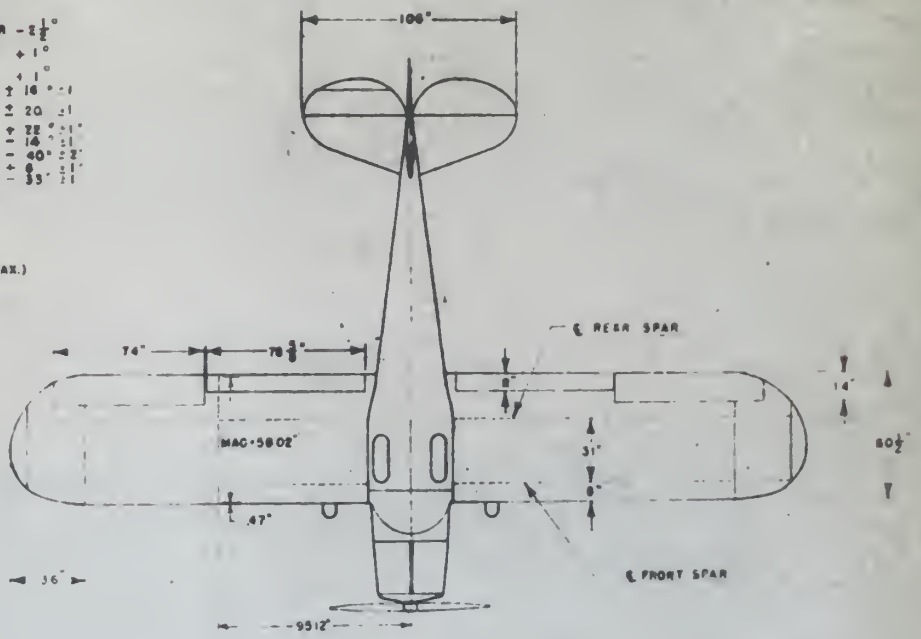

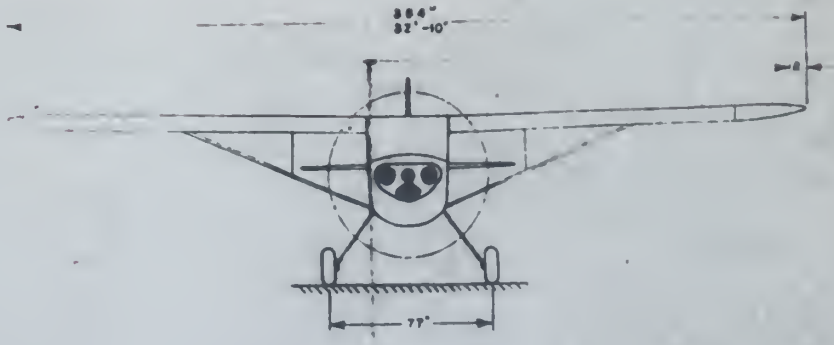

C40000

FIGURE 1. - DISASSEMBLED MODEL

FIGURE 2. - COMPLETE MODEL

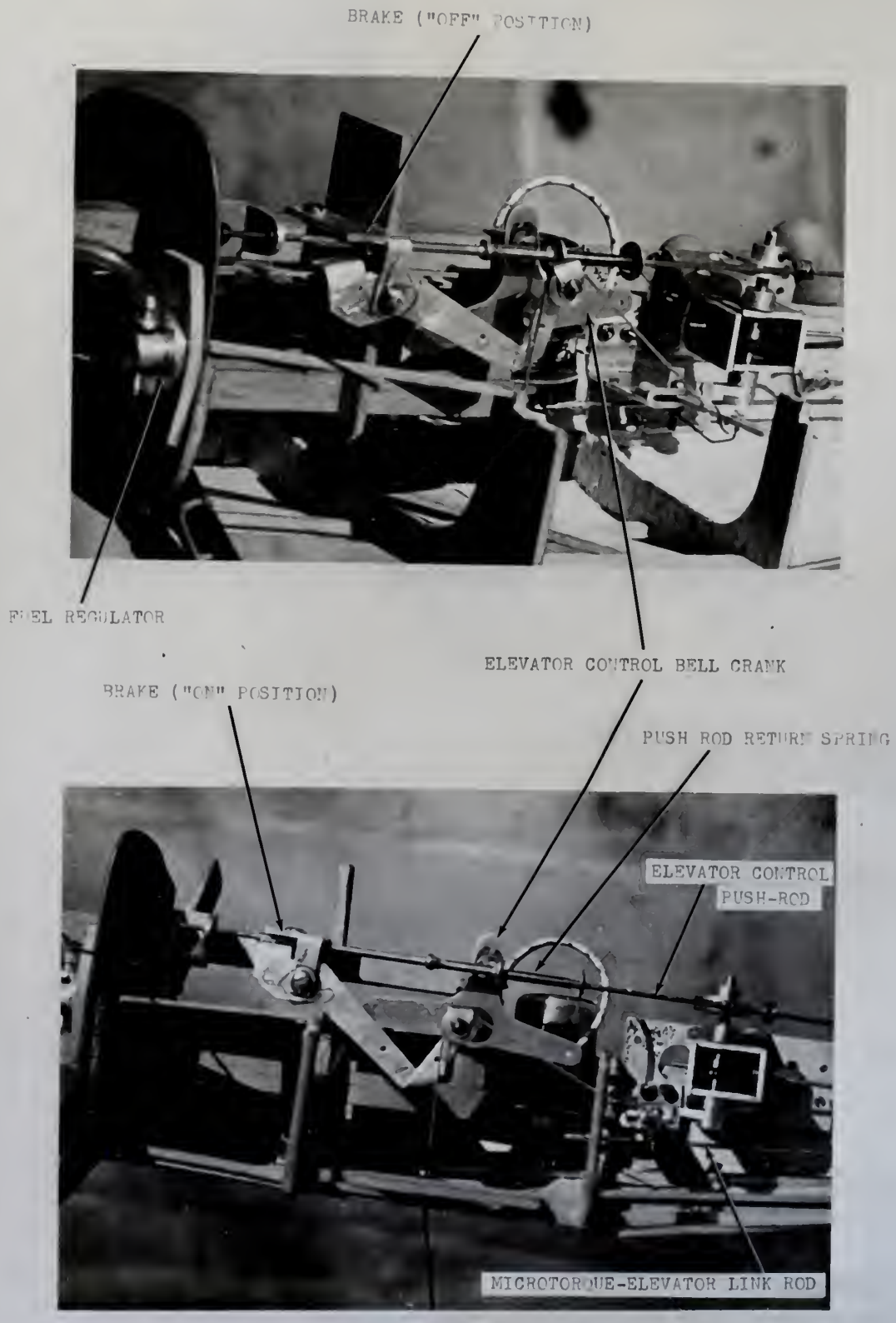

FIGURES 4a, 4b.- TOP VIEWS BEFORE ASSEMBLY SHOWING INTERNAL MECHANISMS

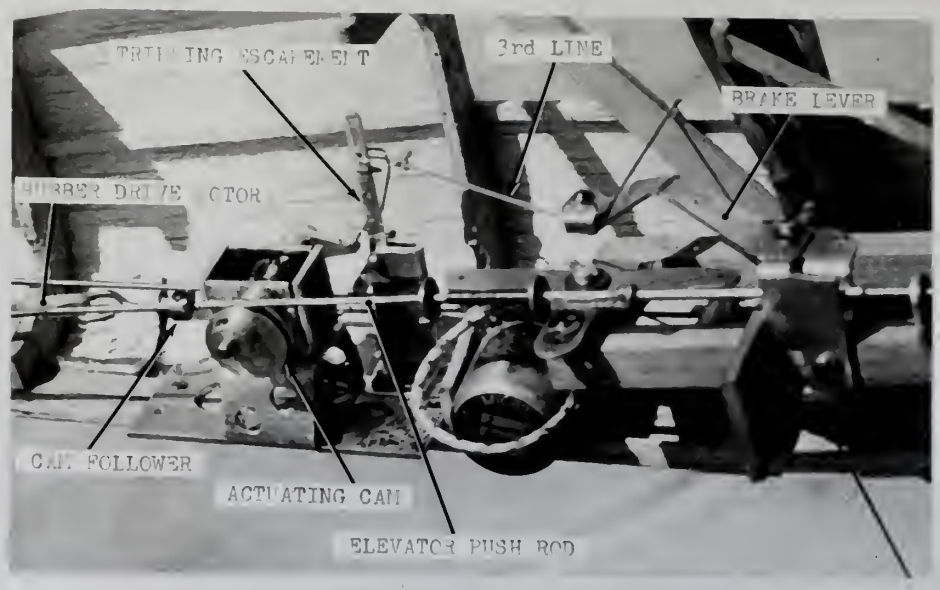

FIGURE 4c. - VIEW FROM RIGHT SIDE BEFORE ASSEMBLY

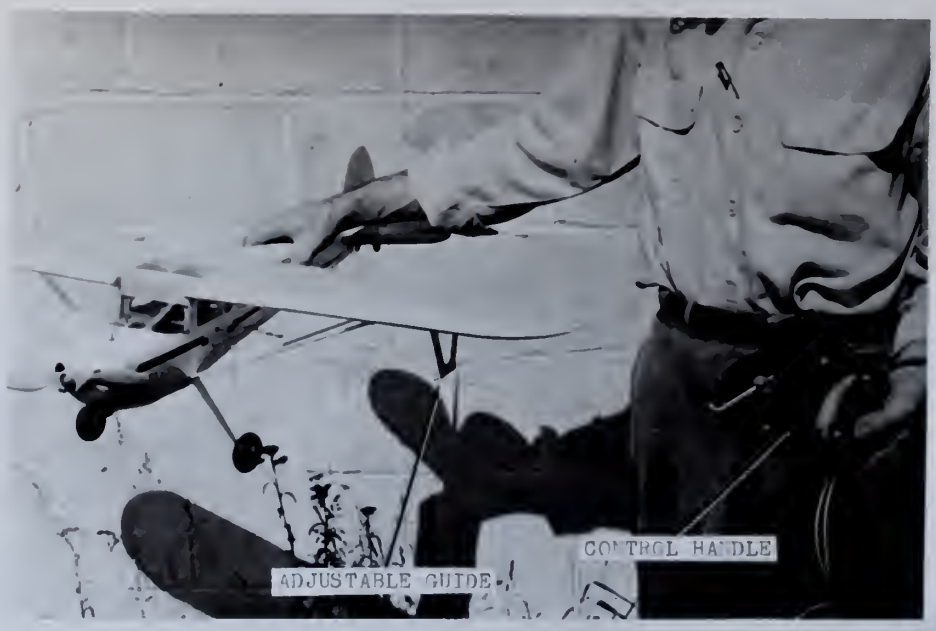

FIGURE 4d. - SHOWING PRIMARY CONTROL WIRES AND CONTROL HANDLE

FIGURE 4e. - SHOWING METHOD OF WINDING RUBBER MOTOR OF ELEVATOR PULSING MECHANISM

FIGURE 4f. - [illegible]

DETAILS OF MEASURING APPARATUS

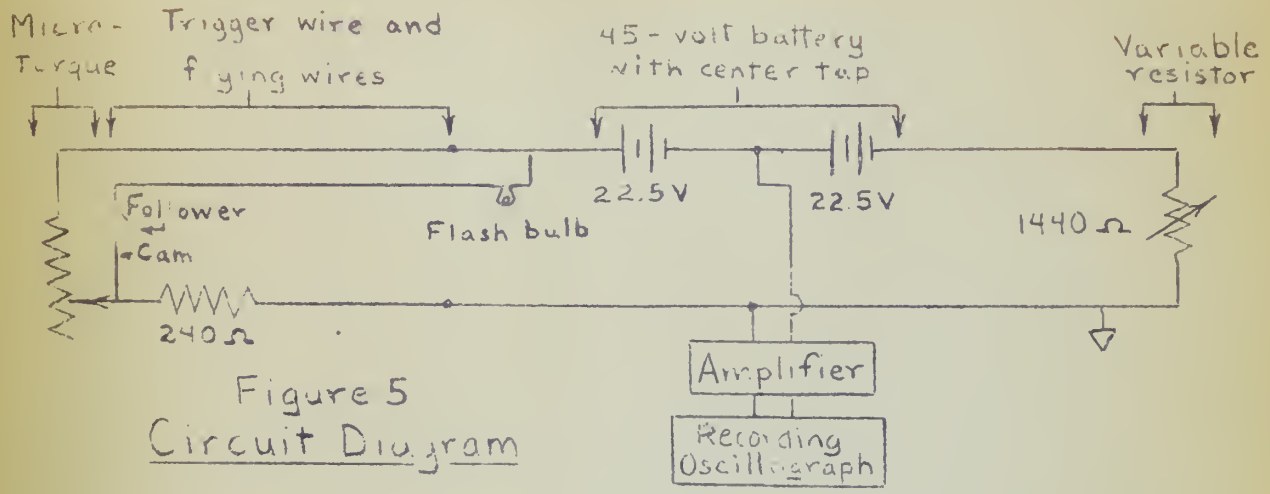

Figure 5
Circuit Diagram

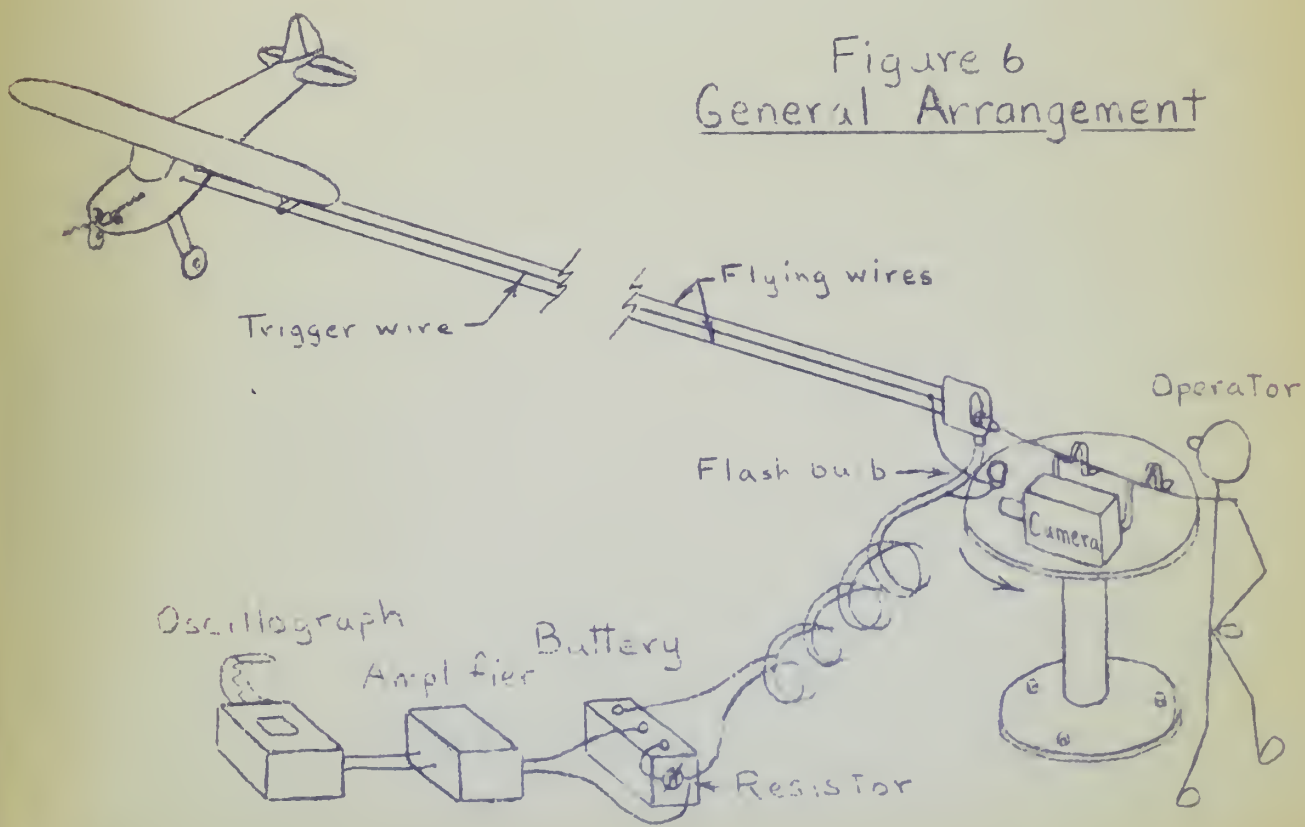

Figure 6
General Arrangement

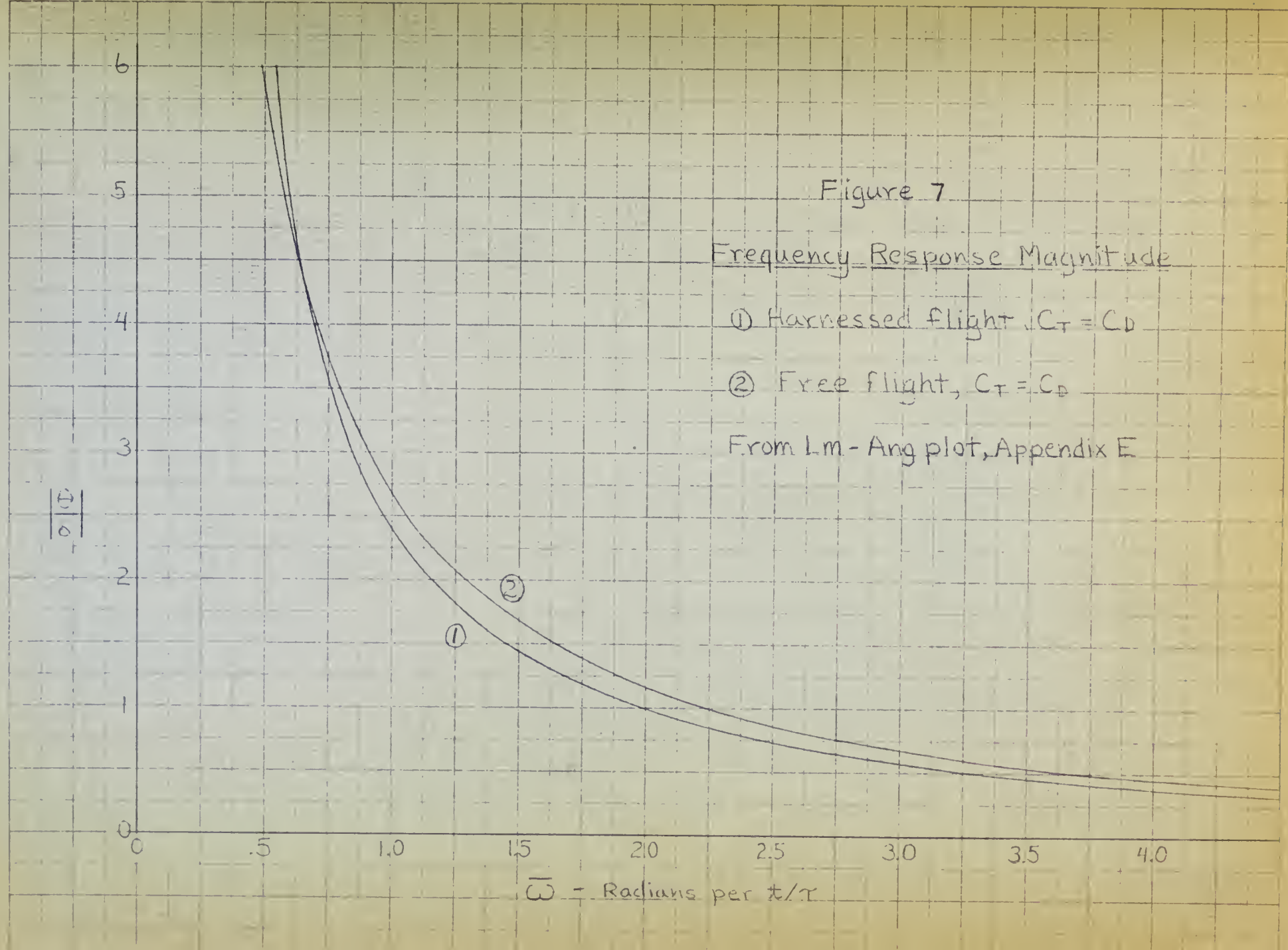

Figure 7

Frequency Response Magnitude

① Harnessed flight, $C_T = C_D$

② Free flight, $C_T = C_D$

From Lm - Ang plot, Appendix E

Figure 7

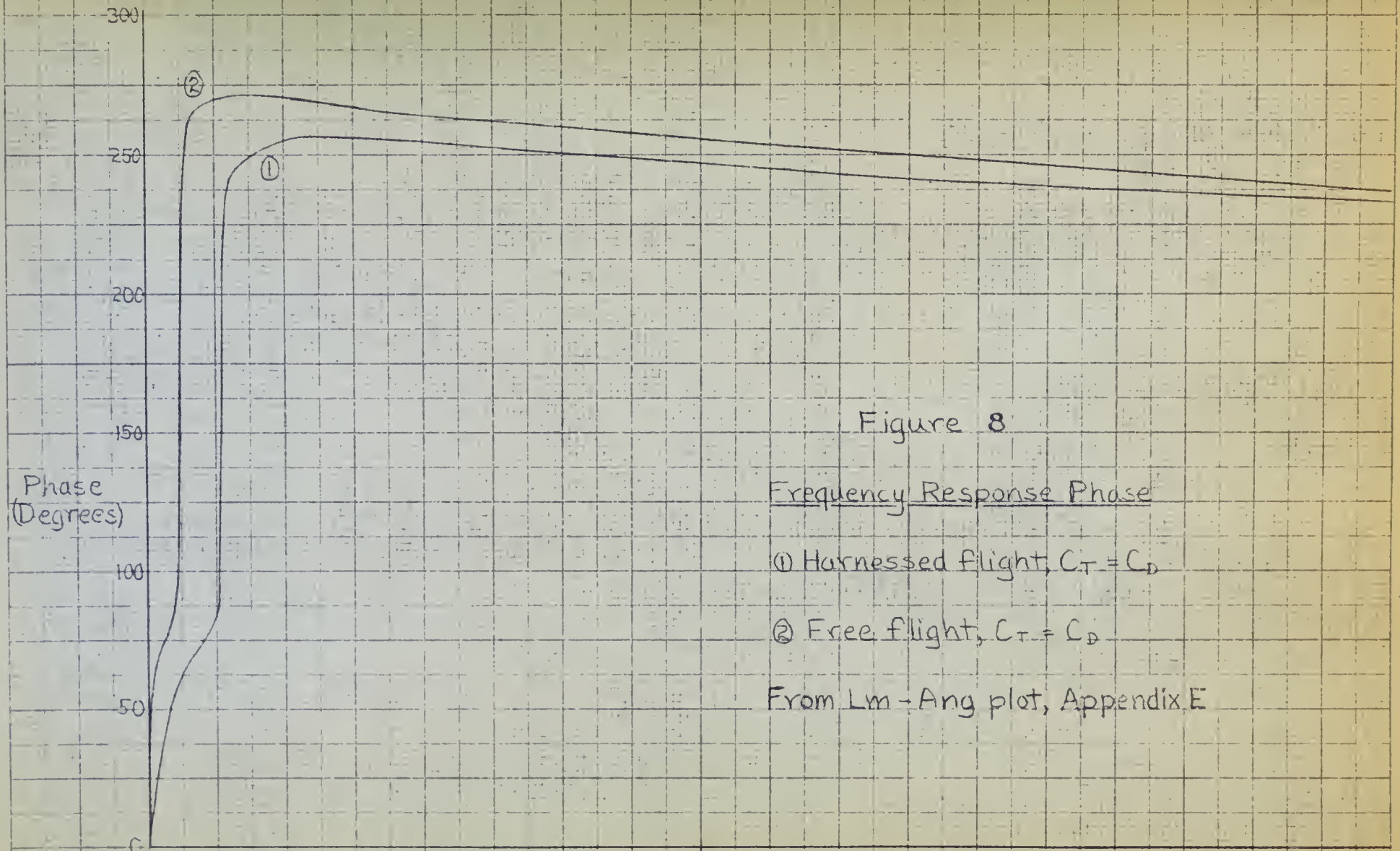

Figure 8

Frequency Response Phase

① Harnessed flight, $C_T = C_D$

② Free flight, $C_T = C_D$

From Lm - Ang plot, Appendix E

Figure 8

Figure 9

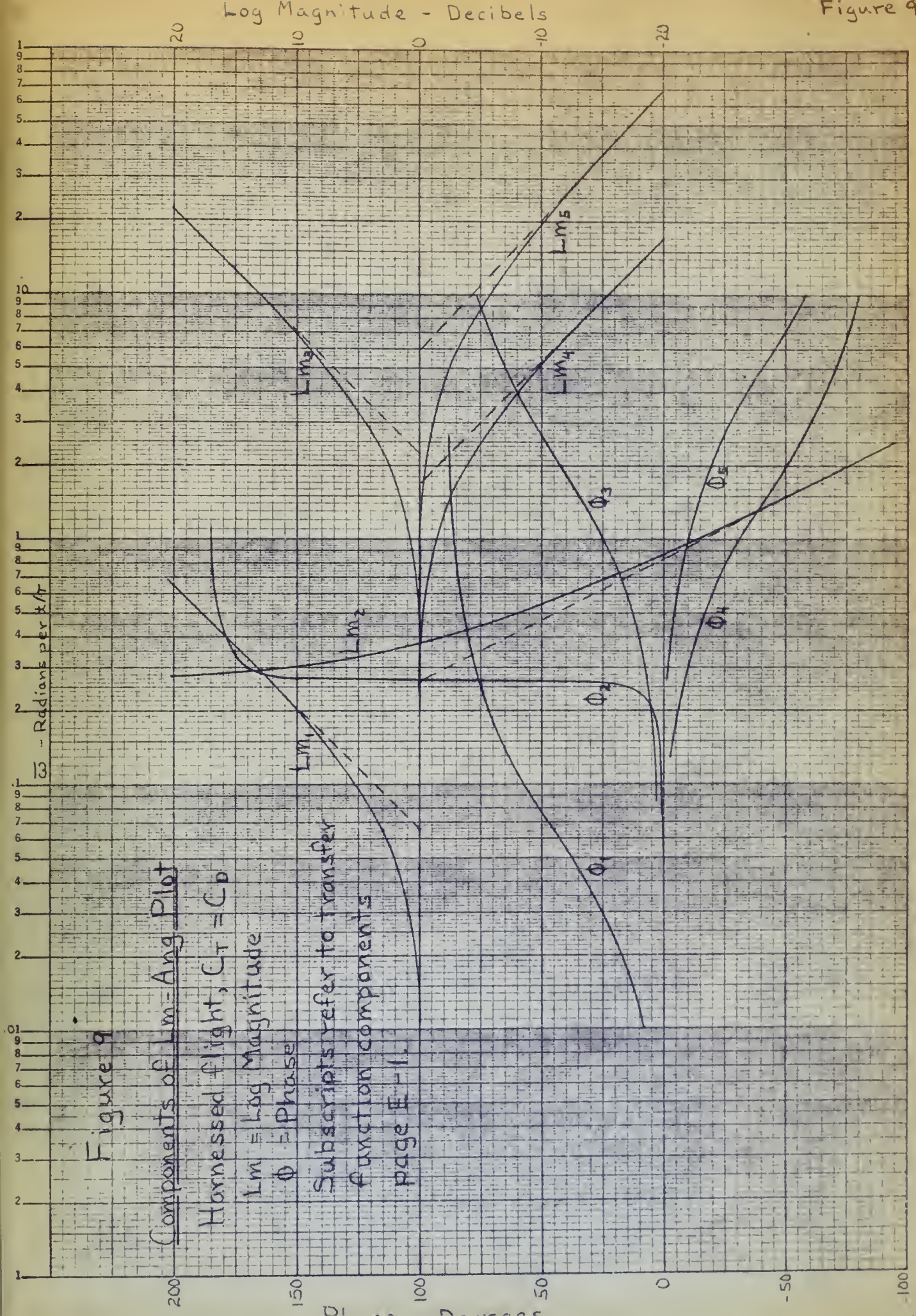

Figure 9
Components of Lm=Ang Plot
Harnessed flight, $C_T = C_D$
Lm = Log Magnitude
Φ = Phase
Subscripts refer to transfer function components
page E-11.

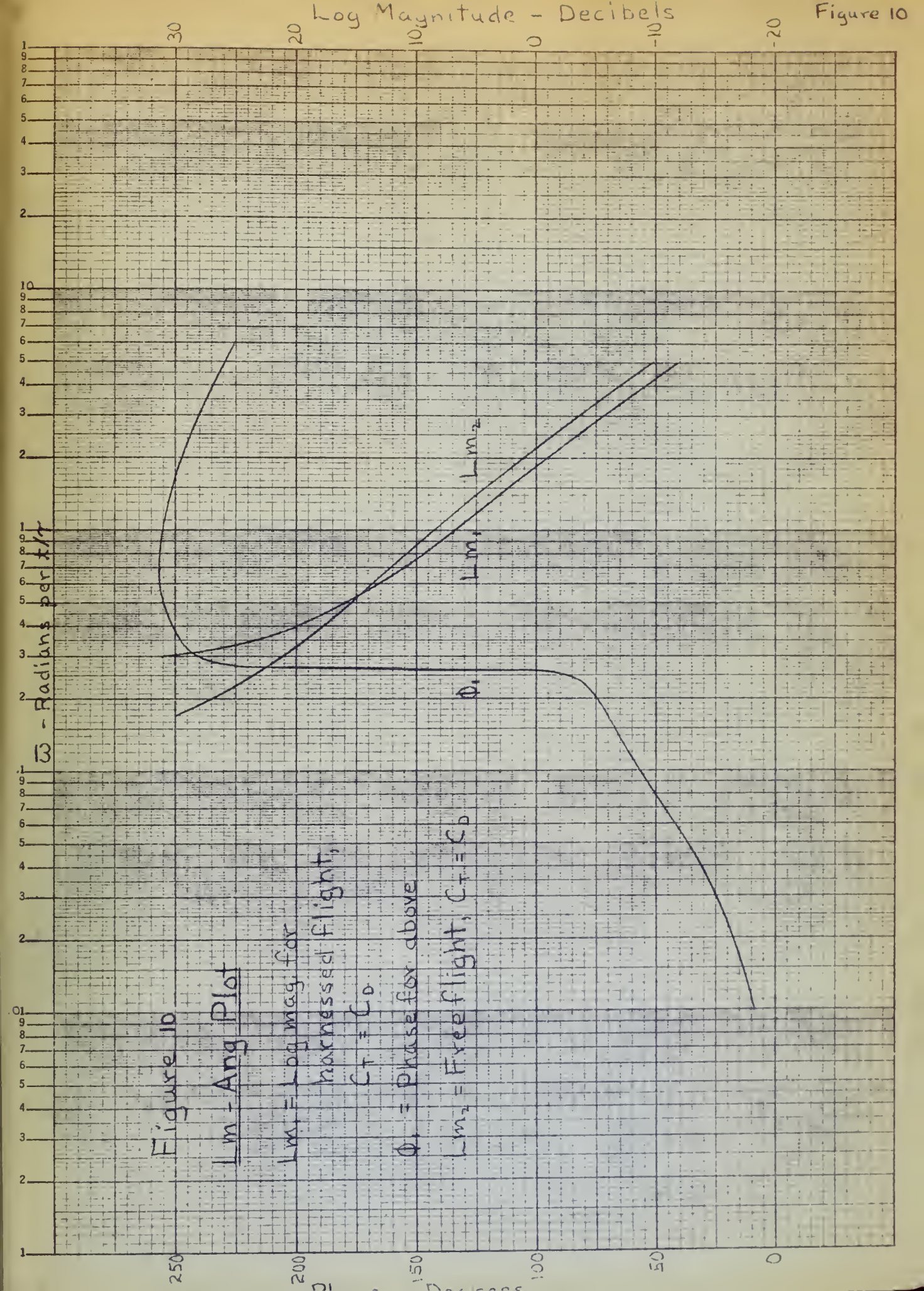
Log Magnitude - Decibels
Figure 10
30
20
10
0
-10
-20
13 - Radians per t/T
250
200
150
100
50
0
Figure 10
Lm - Ang Plot
Lm, = Log mag for
harmessed flight,
$C_T = C_D$
Φ_1 = Phase for above
Lm_2 = Free flight, $C_T = C_D$
Φ_1
Lm_1
Lm_2

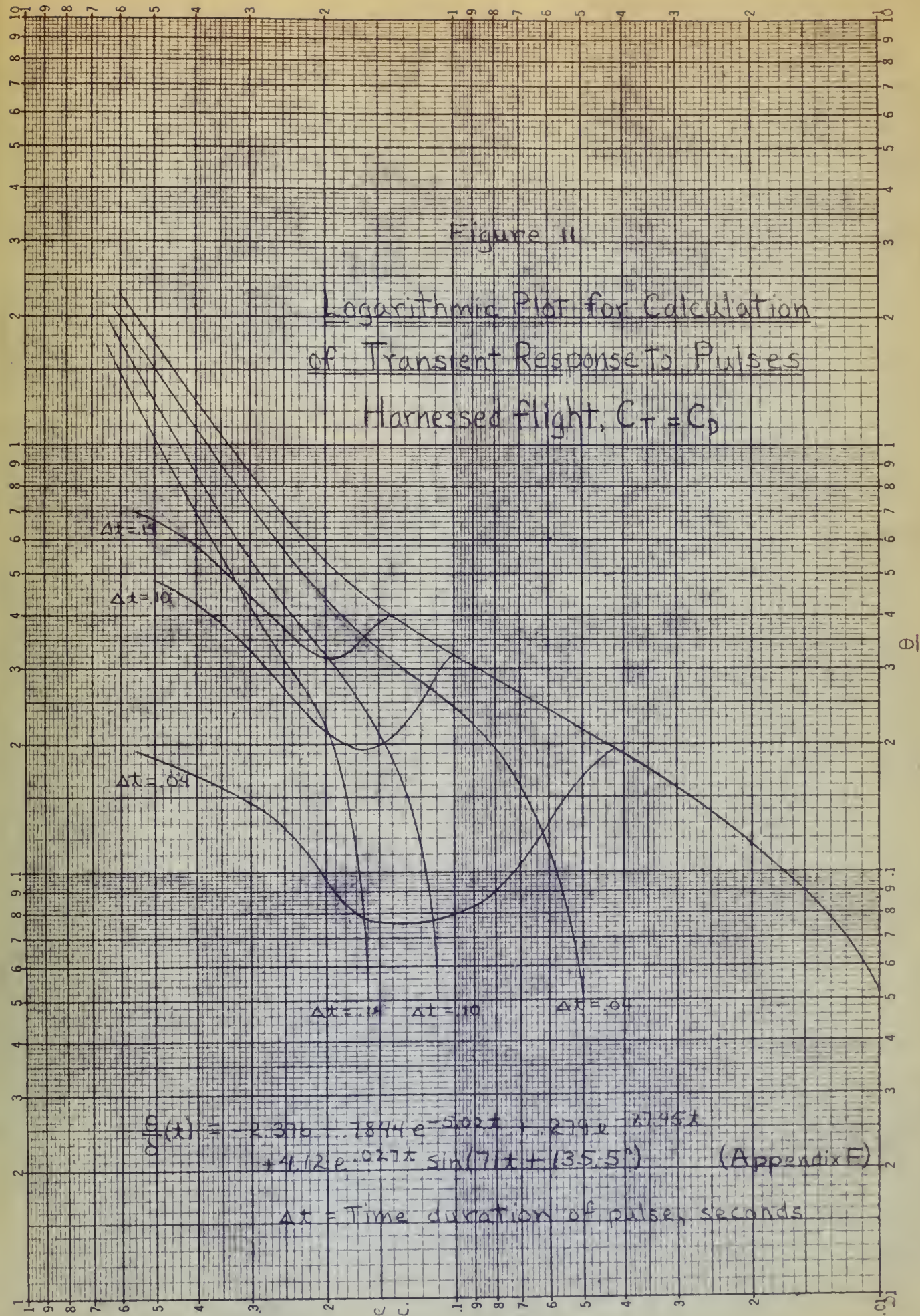
Figure 11
Logarithmic Plot for Calculation
of Transient Response to Pulses
Harnessed flight, $C_T = C_D$
$\Delta t = .14$
$\Delta t = .10$
$\Delta t = .04$
$\frac{\theta}{\delta}(t) = -2.376 - .7844 e^{-.502t} + .279 e^{-.745t}$
$+4.12 e^{-.027t} \sin(.71t + 135.5°)$ (Appendix F)
Δt = Time duration of pulse, seconds

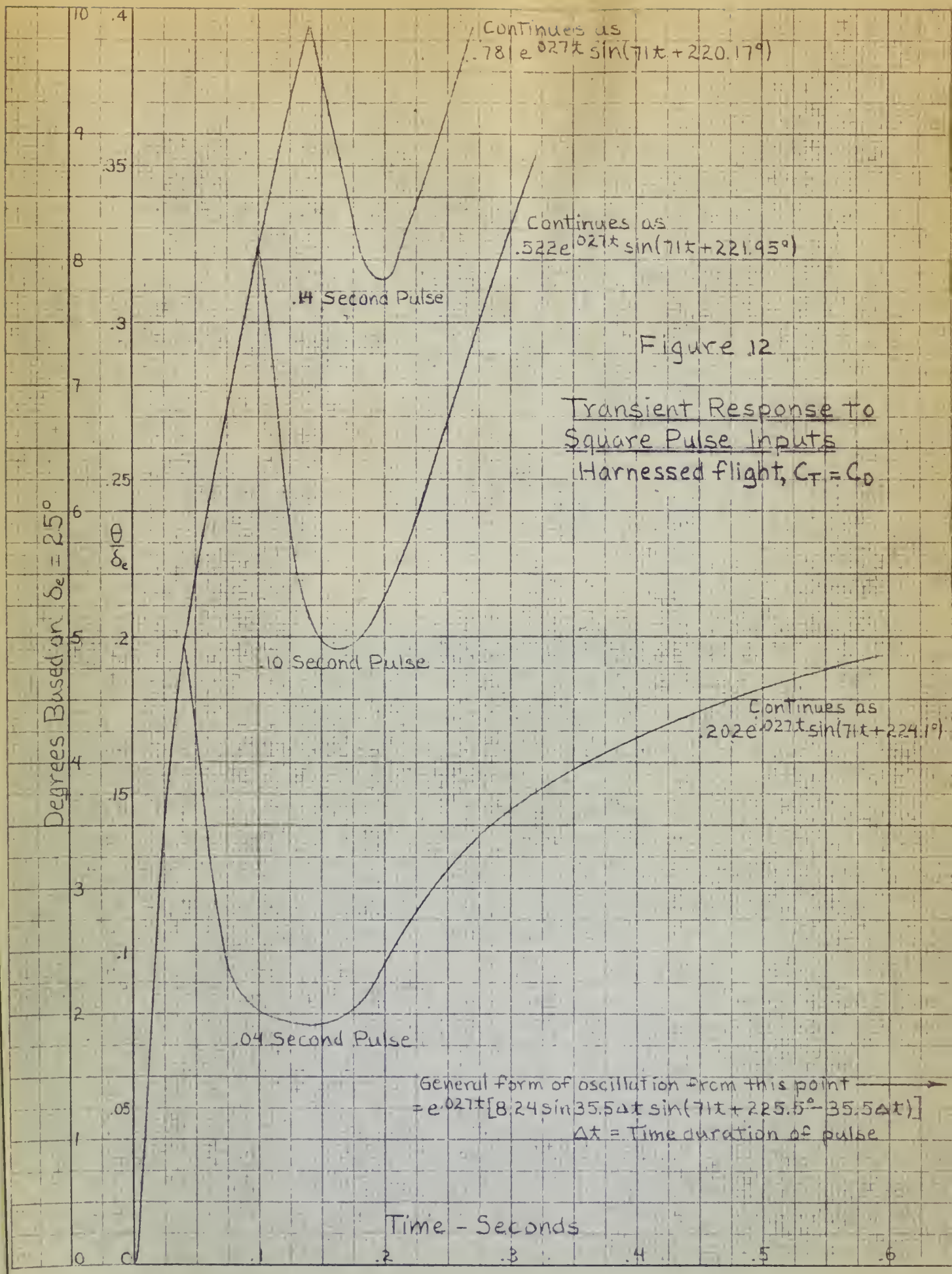

Figure 12

Transient Response to Square Pulse Inputs
Harnessed flight, $C_T = C_D$

Thesis 16269
M93 Munk
Investigation of the feasibility
of using models in harnessed circling
flight for the evaluation of air-
plane longitudinal stability